CHAPTER 4. RESULTS AND DISCUSSION

4.1. CHARACTERISATION OF OVERLOADING AT THE SINKS

In order to elucidate on the spigot loading and overloading behaviour of the dense medium cyclone, a number of parameters were studied during the transition to roping. Spigot loading (in l/hr of both slurry and ore) and the volumetric percentage of ore in sinks were monitored during the transition. Spigot overloading is often associated with the misplacement of sinks particles to the floats stream, hence, the amount of silica particles exiting through the floats stream were also monitored. Medium behaviour within the cyclone during spigot overloading was also investigated by monitoring the medium flow (at both the floats and sinks) and the density differential.

The loading and overloading behaviour of the cyclone was characterized for three spigot sizes of 20, 34 and 45mm diameters; the results are given in Tables A.2, A.3 and A.4 (in Appendix A), respectively. The transitional point between spray and semi-rope discharge, and semi-rope and rope discharge were determined experimentally for the 45mm spigot only.

4.1.1. Spigot Loading

Three types of discharges were observed at the sinks depending on the ore concentration within the cyclone, especially at the sinks. At low concentrations a spray discharge was observed at the sinks (Fig. 4.1), a semi-rope discharge was observed at intermediate concentrations (Fig. 4.2) and a rope discharge was encountered at high ore concentrations (Fig. 4.3).

(a) **(b)**

Figure 4.1. Spray discharge at the sinks for the (a) 165mm cyclone, and (b) 350mm cyclone.

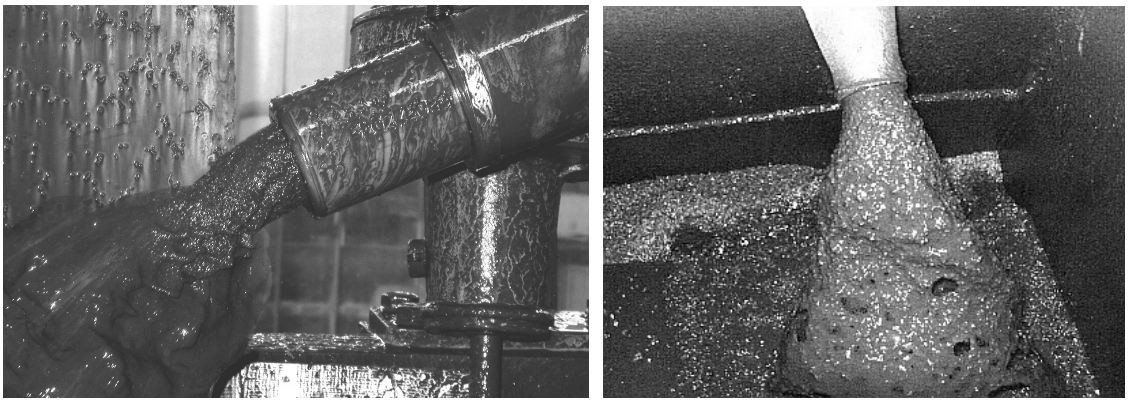

(a) **(b)**

Figure 4.2. Semi-rope discharge at the sinks for the (a) 165mm cyclone, and (b) 350mm cyclone.

During semi-roping the flow at the sinks switched continuously between spray and rope discharges; being mostly spray discharge close to about 11% feed ore concentration and predominantly rope discharge at around 21% (Fig. 4.4). This continuous change between spray and rope discharges during semi-roping is shown in Fig. 4.2, where the flow was in the process of switching to roping from a spray discharge.

(a) **(b)**

Figure 4.3. Rope discharge at the sinks for the (a) 165mm cyclone, and (b) 350mm cyclone.

As expected an increase in the feed ore concentration resulted in increased spigot loading, and the relationship appears to be linear (Fig. 4.4). This linear relationship was observed when spray and semi-rope discharges prevailed at the sinks. However, as soon as the sinks stream changed to roping flow further increase in the feed ore concentration did not result in an increase in spigot loading. Instead the spigot loading remained constant and the spigot appeared to have reached its maximum ore carrying capacity! It can therefore be concluded with certainty that the maximum spigot capacity is reached at the onset of rope discharge at the sinks.

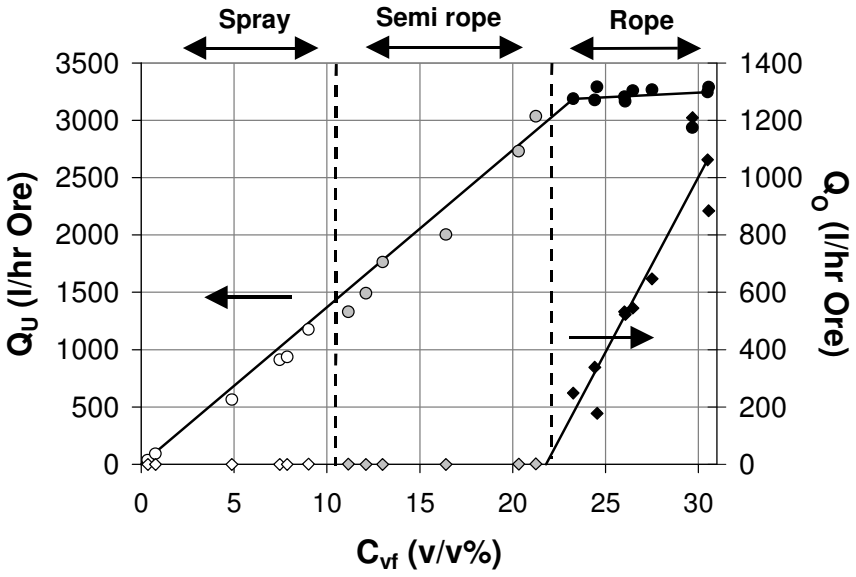

Figure 4.4. Changes in the ore loading at both the floats and sinks streams as ore was added into the cyclone for a 45mm spigot. Data points with white and grey backgrounds were obtained during spray and semi-rope discharges, respectively. While data points with black background were obtained during roping.

The onset of roping flow was also observed to be the point at which silica particles, which were supposed to exit at the sinks stream, were indiscriminately misplaced to the floats stream. The particle size distribution of the silica particles misplaced to the floats stream was exactly the same as that in the sinks stream. This particle misplacement is obviously detrimental to the separation efficiency achieved in the cyclone. Upadrashta and Venkateswarlu (1982) also reported particle misplacement to the floats stream during roping. They proposed the following relationships:

$$S \propto (1 - C_V)^{-0.18} \quad \text{(Spray discharge), and}$$

$$S_R \propto (1 - C_V)^{1.1} \quad \text{(Rope discharge).}$$

The increase in S with increasing C_V during spray discharge was explained to be a consequence of the reduction of the air core size at the sinks, which results in an increase in the proportion of feed material exiting through the spigot. While, on the other hand, the decrease in S_R with increasing C_V during rope discharge is a consequence of misplacement of the sinks particles to the floats stream due to the overloading of the spigot.

It is interesting to note that the misplacement of ore to the floats stream did not actually begin during semi-roping flow, but rather at the commencement of rope discharge. When spray and semi-rope discharges prevailed at the sinks some silica particles of very small quantities were observed to exit at the floats. It is thought this behaviour was due to the probabilistic nature of cyclones.

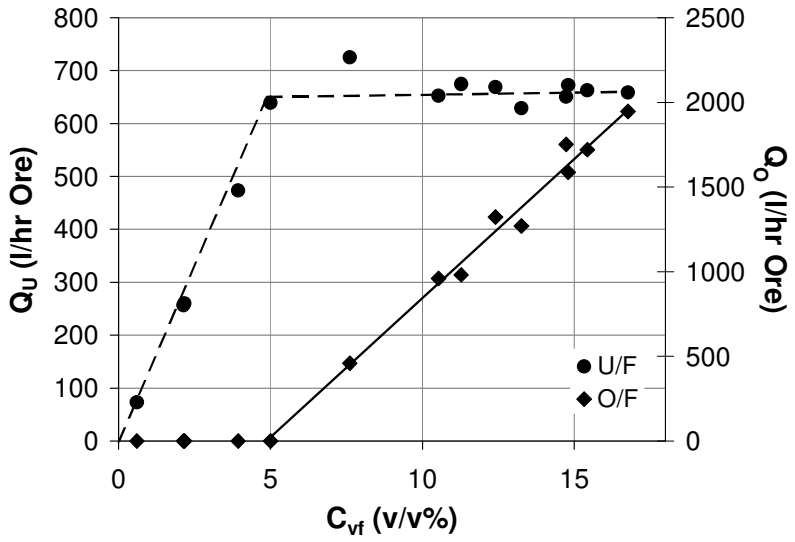

Figure 4.5. Changes in the ore loading at both the floats and sinks streams as ore was added into the cyclone for a 34mm spigot.

Fig. 4.5 and 4.6 show the spigot and vortex finder loading (in l/hr ore) behaviour during the transition to rope discharge for the smaller 25 and 34mm spigots as the feed ore concentration was increased. The point at which the flow changed from spray to semi-rope discharge was not determined for these spigot sizes during the experiments; the same is true for the point of transition to rope discharge. However, just as in Fig. 4.4 above the transitional point from semi-roping to roping flow was easily identifiable from the figure: as soon as roping commenced the spigot loading (in l/hr of ore) did not increase further, and silica particles were misplaced to the floats stream.

Table 4.1 The feed ore concentrations at which roping commenced for the various spigot sizes

D_u (mm)	**C_{vf} at which roping commenced (v/v%)**
25	~3
34	~5
45	~22

Extrapolation of the curve describing the increase in the floats loading during roping, down to the point at which misplacement of the silica particles began appears to give a reasonable estimation of the feed concentration at which roping commenced. The (estimated) feed concentrations at which roping commenced for the 25mm, 34mm and 45mm spigots are shown in Table 4.1. Scrutiny of Fig. 4.4, 4.5 and 4.6 reveals that the feed ore concentration at which roping flow commenced decreased with decreasing spigot size. The spigot capacity is also observed to decrease with decreasing spigot size, however, this will be discussed in more detail later in this chapter.

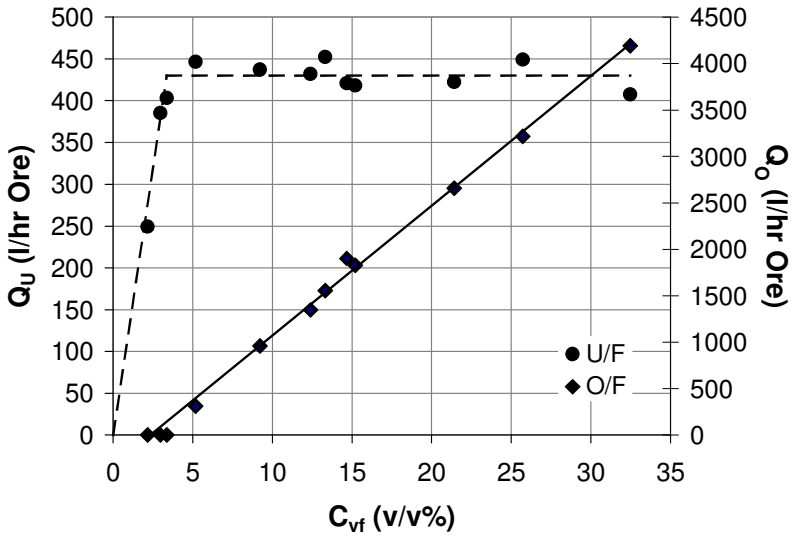

Figure 4.6. Changes in the ore loading at both the floats and sinks streams as ore was added into the cyclone for a 25mm spigot.

The volumetric recovery of both ore to sinks during the transition to roping is shown in Fig. 4.7. All of the ore was recovered in the sinks during spray and semi-rope discharges. Once roping commenced at the sinks there was a reduction in the recovery of ore to sinks, obviously due to ore misplacement to the floats. The feed concentrations at which roping commenced can also be determined from Fig. 4.7.

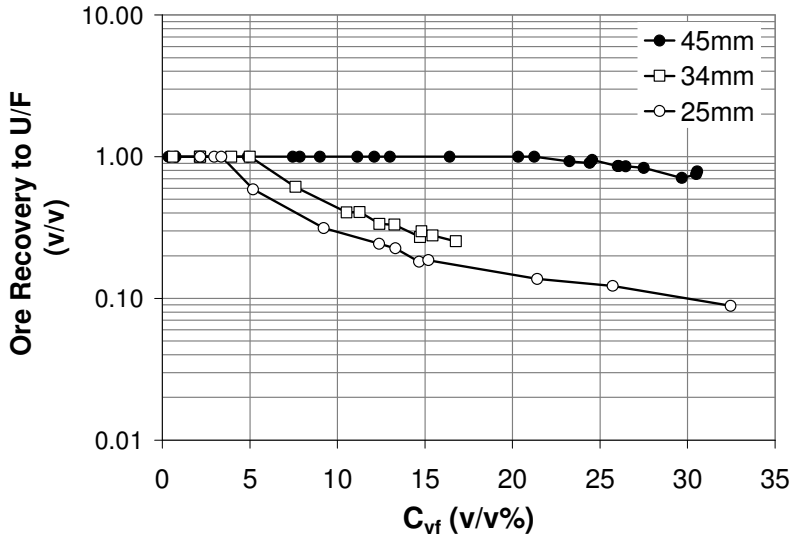

Figure 4.7. Volumetric recovery of ore to sinks during the transition to roping for various spigot diameters.

4.1.2. The Sinks Ore Concentration

The data points obtained during semi-rope discharge were more erratic than those for spray and roping discharge (Fig. 4.8); this behaviour was due to the continuous change in the discharge types at the sinks between spray and rope discharges. The transition from a semi-rope to a rope discharge resulted in a sharp increase in C_{vu}.

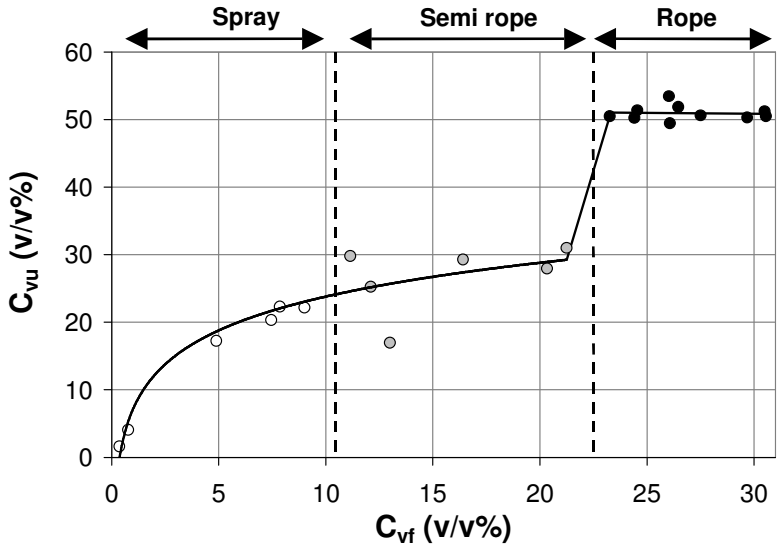

Figure 4.8. The volumetric ore concentration at the sinks for a 45mm spigot. Data points with white and grey backgrounds were obtained during spray and semi-rope discharges, respectively. While data points with black background were obtained during roping.

It was not possible in this study to maintain sinks ore concentrations at values between approximately 31 to 50% for the 45mm spigot; as soon as the ore concentration exceeded about 31% roping commenced. It is thought that this behaviour does not necessarily represent the behaviour of all cyclones. Under overloaded conditions, the sinks ore concentration remained constant at around 50% (for the 45mm spigot) with further increases in the feed ore concentration. It is clear from Fig. 4.8 that the onset of spigot overloading can be anticipated by monitoring C_{vu}. Stas (1957) too observed that when the spigot was overloaded the sinks ore concentration remained constant with further increases in the feed ore concentration. Alternatively C_{vu} could be expressed in terms of volumetric medium-to-ore ratio, which is common practice in industry. Fig. 4.8 in terms of medium-to-ore ratio is shown in Fig. 4.9. During roping the volumetric medium-to-ore ratio at the sinks was generally around 1:1 (for the 45mm spigot).

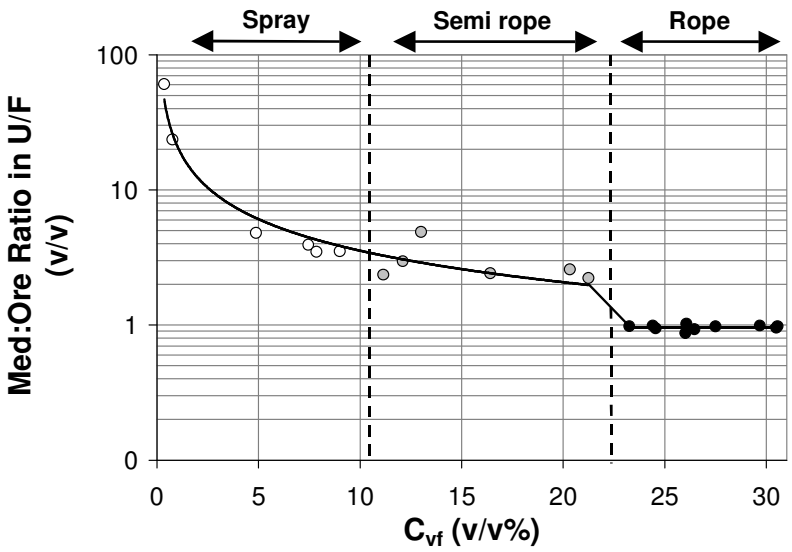

Figure 4.9. The volumetric medium-to-ore ratio at the underflow for a 45mm spigot. Data points with white and grey backgrounds were obtained during spray and semi-rope discharges, respectively. While data points with black background were obtained during roping.

It is not clear whether the presence of coal particles (floats) in the floats stream would change the nature of the relationship between the feed and sinks concentrations as shown in Fig. 4.8. The presence of floats particles in the floats stream is, however, not expected to significantly change the critical sinks ore concentration at which roping is encountered. A regression of Fig. 4.8 during spray and semi-rope discharges gives the following expression:

$$C_{vu} = n \ln[C_{vf(+\rho_{50})}] + k \qquad (4.1)$$

with n = 7.223 and k = 7.165, and R^2 = 0.981. C_{vu} is the volumetric percentage of ore in the sinks stream during spray and semi-roping, and $C_{vf(+\rho 50)}$ is the volumetric percentage of ore in the feed with densities above the cut density at which the cyclone is operating at. It is expected that parameters n and k should change with changes in the cyclone geometry and operating conditions. Note that the two data points that appear to be outliers at semi-roping regime in Fig. 4.8 were not considered in obtaining the above expression. This expression describes how C_{vu} increases with increasing $C_{vf(+\rho 50)}$, for the conditions under which these tests were performed. It does not take into account the onset of roping, thus, prior knowledge of the $C_{vf(+\rho 50)}$ (at which the abrupt jump in C_{vu} occurs) at the onset of roping is required.

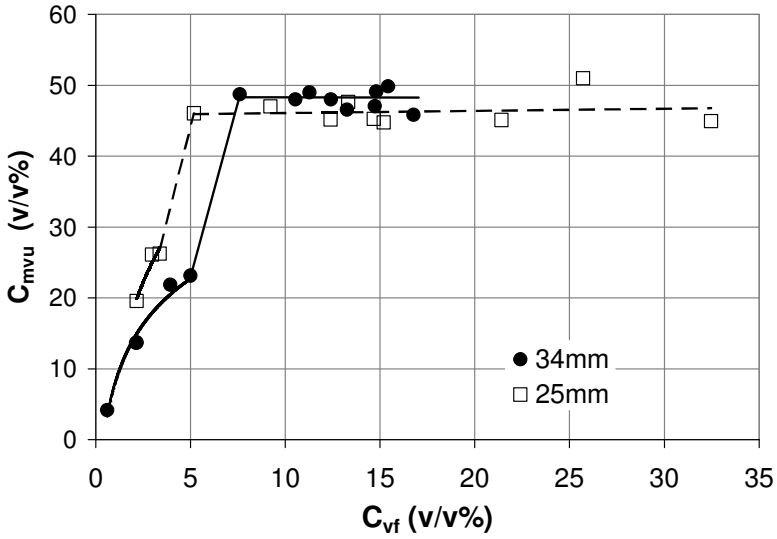

Figure 4.10. The volumetric ore concentration at the sinks for the 25 and 34mm spigots.

Fig. 4.10 shows the change in C_{mvu} with increasing feed concentration during the transition to rope discharge for the 25 and 34mm spigots. The manner in which C_{vu} changed with increasing feed concentration for the 25 and 34mm spigots confirms the results shown in Fig. 4.8. Further, Fig. 4.8 and 4.10 illustrate that C_{mvu} decreased with decreasing spigot size. The decrease in the concentration was, however, relatively small. C_{mvu} values obtained with the 25 and 34mm spigots expressed in terms of volumetric medium-to-ore ratios are shown in Fig. 4.11.

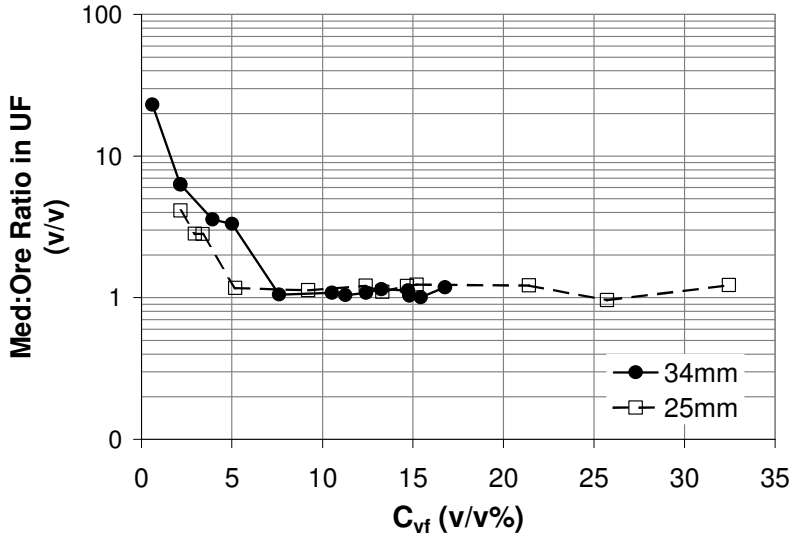

Figure 4.11. The volumetric medium-to-ore ratio at the sinks for the 25 and 34mm spigots during the transition to roping.

The increase in C_{vu} with increasing C_{vf} during spray and semi-rope discharges, for the smaller 25 and 34mm spigots, was also according to a relationship of the form of equation 4.1. Table 4.2 shows the parameters *n* and *k*, and the R^2 values for the 25, 34 and 45mm spigots. The fit of the curves to the data was generally good, and the parameter *k* appears to be relatively unaffected by changes in the spigot diameter. While, on the other hand, parameter *n* appears to be dependent on spigot size.

Table 4.2. Parameter values for equation 4.1.

D_u (mm)	Parameter *n*	Parameter *k*	R^2
25	16.092	7.465	0.928
34	9.216	7.915	0.974
45	7.223	7.165	0.981

The range of C_{mvu} values obtained from all the tests performed in this study is shown in Fig. 4.12; C_{mvu} obtained in this study ranged from 43 up to 54% (v/v). The C_{mvu} values of 56 and 57% shown in Fig. 4.12 are thought to be erroneous because repetition of these tests did not reproduce the same results. The same was true for the C_{mvu} value of 41 in Fig. 4.12. The C_{mvu} values in Fig. 4.12 compares very well with the $\%V_{MSU}$ values (for classification cyclones) reported in the literature, which ranged from 39 to 68% (v/v). They are also in good agreement with Clarkson and Wood (1993)'s proposed sinks ore concentration upper limit of 40% (to avoid spigot overloading).

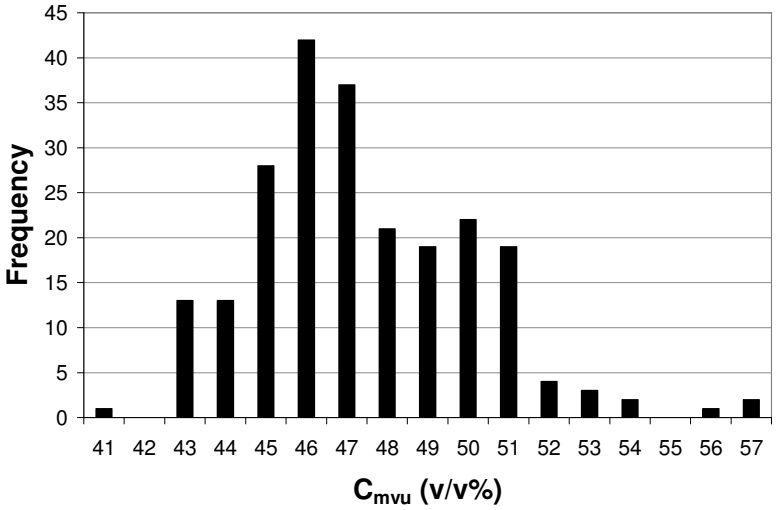

Figure 4.12. Range of all ore concentrations obtained in this investigation when roping was prevalent at the sinks.

Alternatively C_{mvu} can be expressed in terms of volumetric medium-to-ore ratios; the range of sinks medium-to-ore ratios obtained during roping in this study is shown in Fig. 4.13. These ranged mainly from 0.9 to 1.3 (v/v).

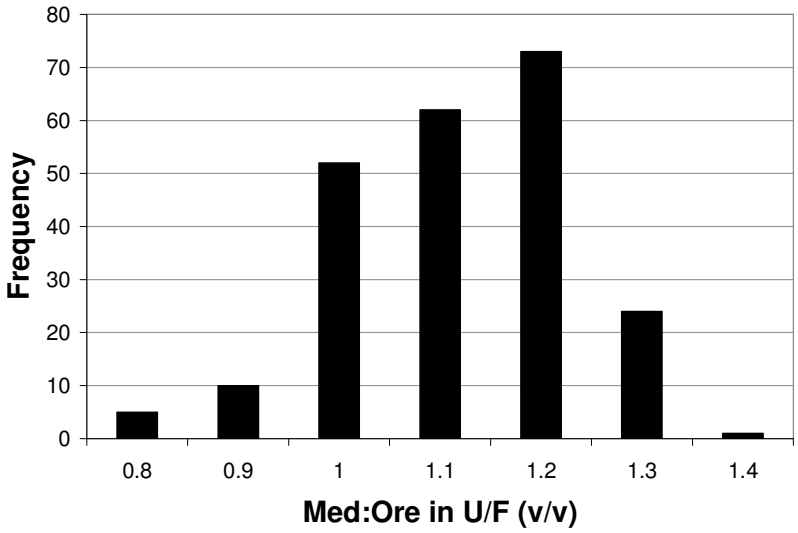

Figure 4.13. Range of all the sinks medium-to-ore ratios obtained in this investigation when roping was prevalent at the sinks.

4.1.3. Slurry Flow

The change in the slurry flow-rate through the 45mm spigot during the transition to roping is shown in Fig. 4.14. The slurry flow-rate at the sinks increased in a similar manner to the ore flow-rate before roping flow commenced (Fig. 4.4 and 4.14). During the transition to roping a drastic drop in the slurry flow-rate occurred, after which the flow-rate remained constant with further addition of ore into the cyclone. The ore flow-rate did not change abruptly during this transition (Fig. 4.4), thus, the abrupt drop in slurry loading at the sinks was a consequence of changes in the behaviour of medium flow which also dropped sharply during the transition to roping (Fig. 4.18). This also accounts for the sudden increase in the sinks ore concentration during the transition to roping flow (Fig. 4.8).

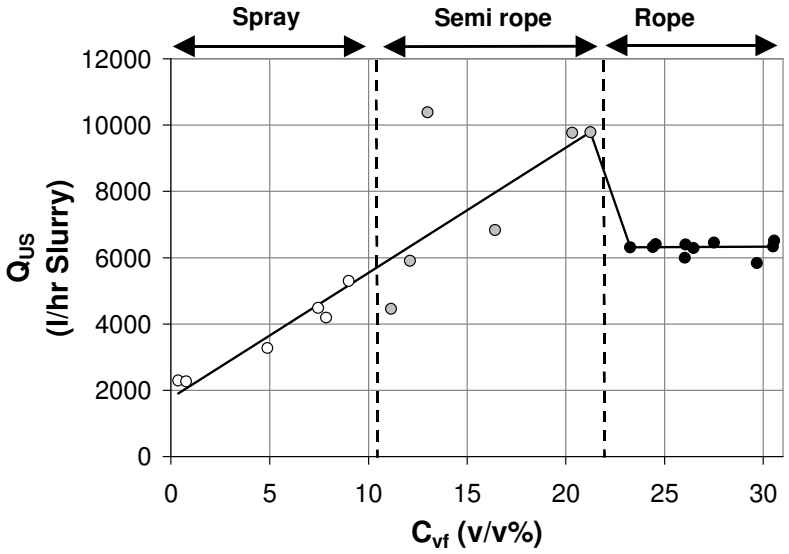

Figure 4.14. Slurry loading at the sinks for the 45mm spigot. Data points with white and grey backgrounds were obtained during spray and semi-rope discharges, respectively. While data points with black background were obtained during roping.

Fig. 4.15 shows the change in the slurry loading at the sinks during the transition to roping flow for the 25 and 34mm spigots. The nature of the influence of the feed concentration on the slurry loading at the spigot for the 25 and 34mm spigot is similar to that of the 45mm spigot reported in Fig. 4.14. It is interesting to note that the slurry flow-rate during roping for the 34mm spigot was below that obtained when only medium was fed into the cyclone. Similarly, the slurry flow-rate during roping for the 25mm spigot was almost equal to that obtained when only medium was fed to the cyclone. This is quite different from the behaviour observed in Fig. 4.14 for the larger 45mm spigot.

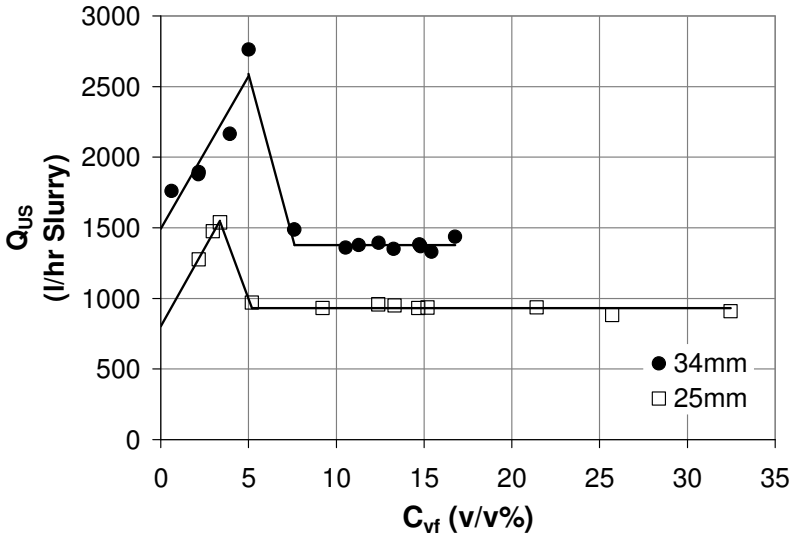

Figure 4.15. Slurry loading at the sinks for the 25 and 34 mm spigot.

Fig. 4.16 shows the influence of increasing feed ore concentration on the cyclone throughput. The slurry throughput through the cyclone increased with increasing feed concentration during spray and semi-rope discharges. Once roping commenced, the throughput decreased with further increase in feed ore concentration. This decrease in the slurry throughput is actually a consequence of the decreasing floats flow-rate during roping; the conditions at the sinks have been established to be constant once roping commences (Fig. 4.4, 4.8 and 4.14). The decrease in the slurry flow-rate at the floats is reflected in the decreasing floats medium flow-rate as shown in Fig. 4.18.

The increase in the ore throughput with increasing feed concentration during spray and semi-rope discharges (Fig. 4.16) is the same as that shown in Fig. 4.4 (for the spigot loading). The ore throughput increase during roping (Fig. 4.16), however, is a reflection of the increase in the ore flow-rate through the floats; the ore flow-rate through the sinks remained constant with further increase in the feed concentration once roping had commenced (Fig. 4.4).

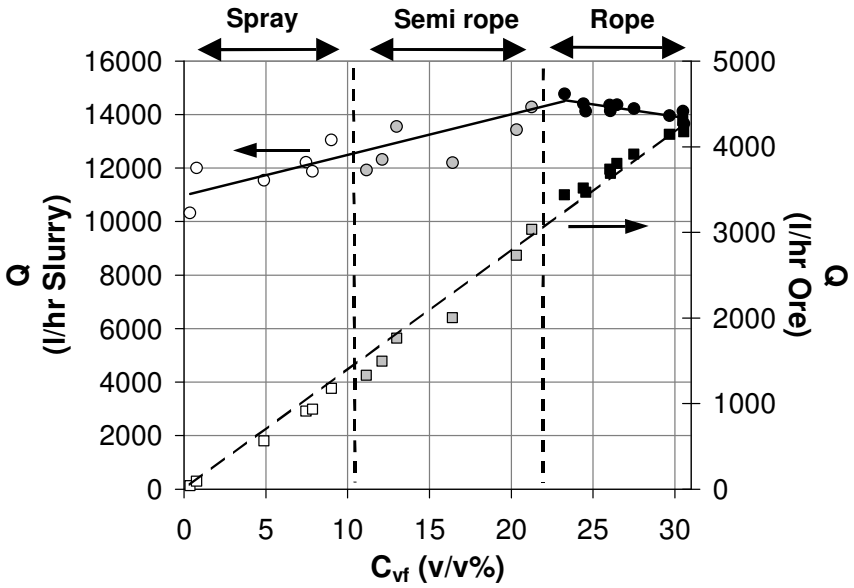

Figure 4.16. Cyclone throughput (both ore and slurry) during the transition to rope discharge for the 45mm spigot. Data points with white and grey backgrounds were obtained during spray and semi-rope discharges, respectively. While data points with black background were obtained during roping.

This decrease in the cyclone slurry throughput with increasing feed concentration during roping (Fig. 4.16) is in agreement with the findings of Upadrashta and Venkateswarlu (1982). They also observed Q to decrease with increasing feed concentration during roping; this behaviour was in accordance with the following relationship:

$$Q \propto (1 - C_V)^{0.56} \quad \text{(Rope discharge)}$$

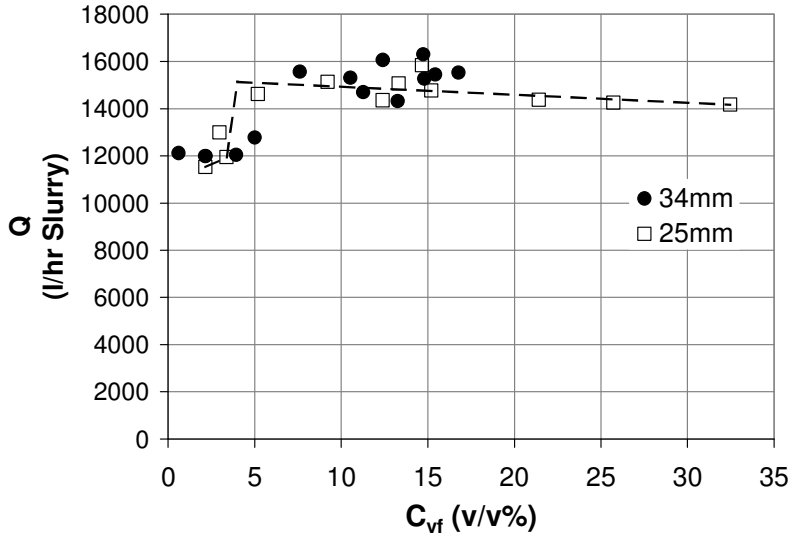

Figure 4.17. Cyclone slurry throughput during the transition to rope discharge for the 25 and 34mm spigots.

A look at the slurry throughput for the 25 and 34mm spigots reveals a different trend (Fig. 4.17): a sharp increase in the slurry throughput was observed at the transition to roping, after which the throughput decreased slightly for the 25mm spigot; the slurry throughput for the 34mm spigot remained relatively constant with further increase in the feed concentration during roping. These results also agree with the findings of Upadrashta and Venkateswarlu (1982). The sudden increase in the cyclone throughput at the onset of roping has also been reported by Plitt et al (1987), who observed a 16% increase in the cyclone flow-rate during the transition to roping.

4.1.4. Medium Flow

During the transition to roping the medium flow-rate at the sinks dropped abruptly, and this coincided with a drastic rise in the medium flow-rate at the floats; indicating that the onset of roping at the spigot resulted in a transfer of medium from the sinks to the floats. The steady drop in medium flow-rate at the floats during roping is a consequence of increased quantities of silica particles that had been misplaced to the floats (Fig. 4.4). Furthermore, there was a transfer of medium from the floats to the sinks with increasing feed ore concentration before roping commenced (Fig. 4.18). This is thought to be a consequence of the interaction between the silica particles and medium, resulting in the 'dragging' of medium to the spigot. This behaviour was also observed by Wood (1990), who observed, "Excessive sinks flow tends to carry additional medium to (sinks stream), rather than displace medium from the (sinks stream)".

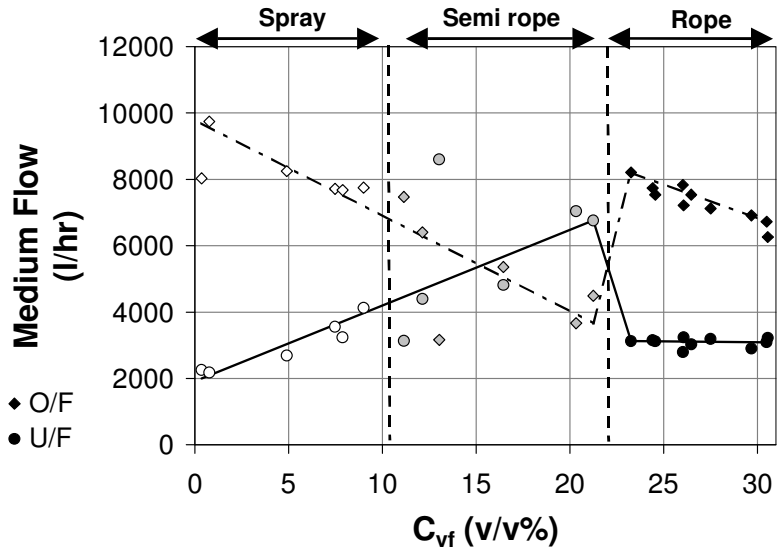

Figure 4.18. Medium flow-rate at the floats and sinks during the transition to rope discharge for the 45mm spigot. Data points with white and grey backgrounds were obtained during spray and semi-rope discharges, respectively. While data points with black background were obtained during roping.

The medium flow-rates at the sinks for the 25 and 34mm spigots during the transition to roping are shown in Fig. 4.19. Again the behaviour for the small spigots (25 and 34mm) mirrors that of the 45mm spigot as shown in Fig. 4.18.

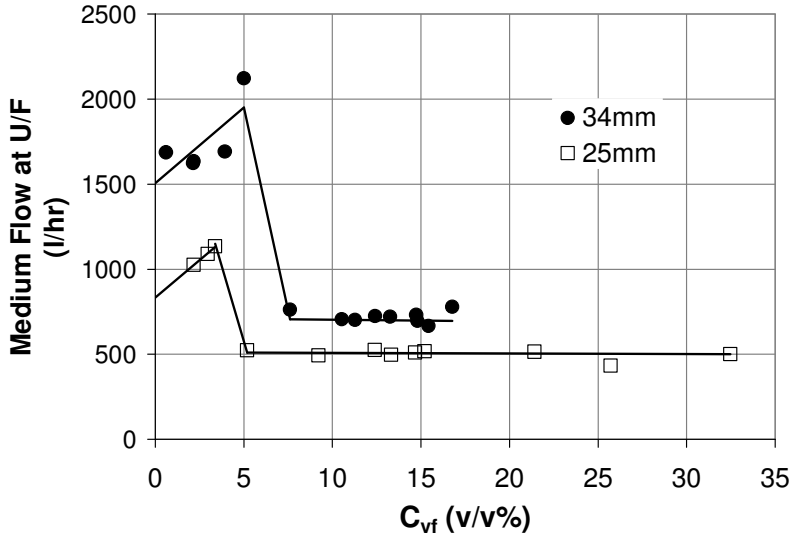

Figure 4.19. Medium flow-rate at the sinks during the transition to rope discharge for the 25 and 34mm spigots.

Fig. 4.20, on the other hand, illustrates the changes in the medium flow-rate at the floats during the transition to roping for the 25 and 34mm spigots.

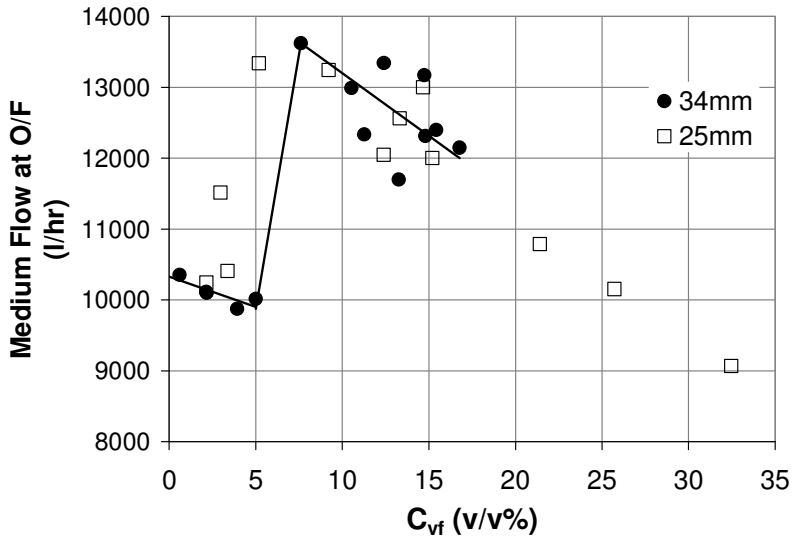

Figure 4.20. Medium flow-rate at the floats during the transition to rope discharge for the 25 and 34mm spigots.

The above-mentioned transfer of medium from the floats to the sinks with increased addition of silica particles into the cyclone, during spray and semi-rope discharges, was further confirmed by the behaviour of the density differential parameter (Fig. 4.23 and 4.24).

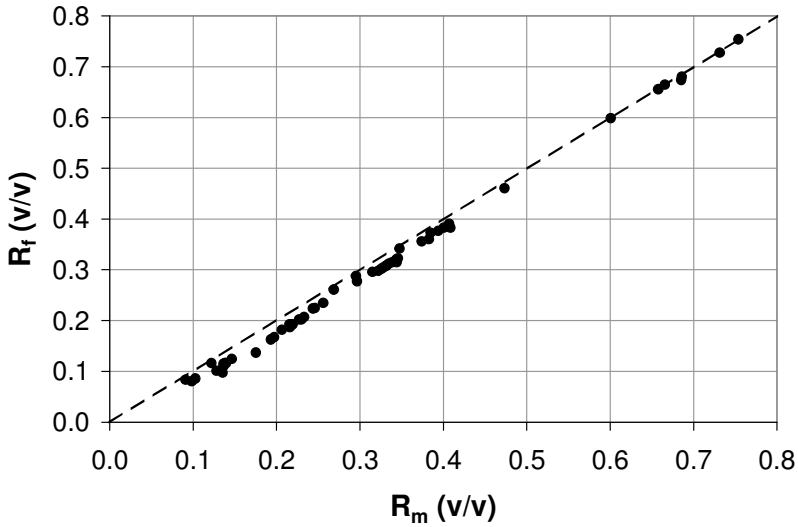

Figure 4.21. The relationship between R_f and R_m when spray and semi-rope discharges were prevalent at the sinks.

Volumetric medium split to sinks (R_m) is illustrated to be very similar to the water split to sinks (R_f) during spray and semi-rope discharges in Fig. 4.21. R_m was consistently higher than R_f at R_f and R_m values below 0.6. The relationship between R_f and R_m during roping is shown in Fig. 4.22, where the R_f and R_m values are almost always equal. The systematic deviation of

R_f from R_m observed during spray and semi-rope discharges was not evident during roping. This is indicative of a stabilized medium during roping conditions.

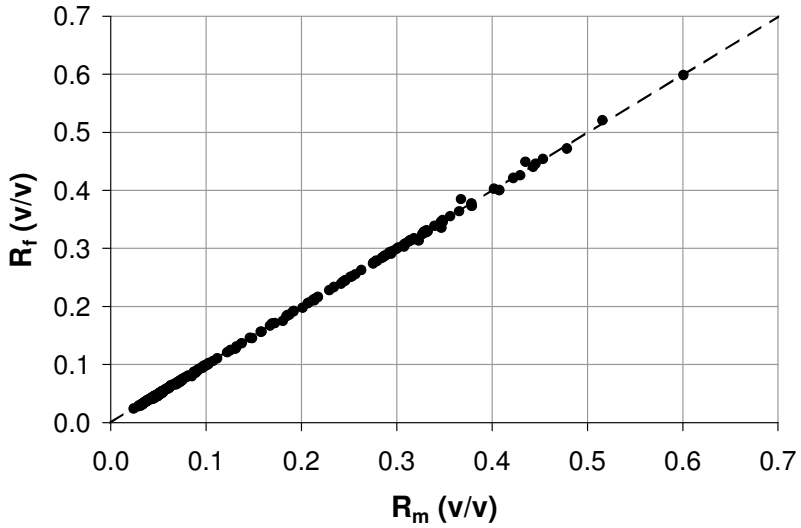

Figure 4.22. The relationship between R_f and R_m when rope discharge was prevalent at the sinks.

4.1.5. Density Differential

Density differential refers to the difference between the sinks and floats medium densities. The decrease in the differential observed in Fig. 4.23 and 4.24 is a consequence of the dilution of the high-density medium at the sinks by the low-density medium from the floats that was carried over to the spigot by the ore particles. According to King and Juckes (1984) when the volumetric medium-to-coal ratio approaches 1:1 the particles interact with each other, and this interaction changes the medium properties. The actual values of the density differentials shown in Fig. 4.23 and 4.24 might change in the presence of floats particles due to the consequent interaction between the floats particles and medium. The trend of the curve in Fig. 4.23 and 4.24 is, however, not expected to change, thus, spigot overloading should always be associated with relatively low-density differentials.

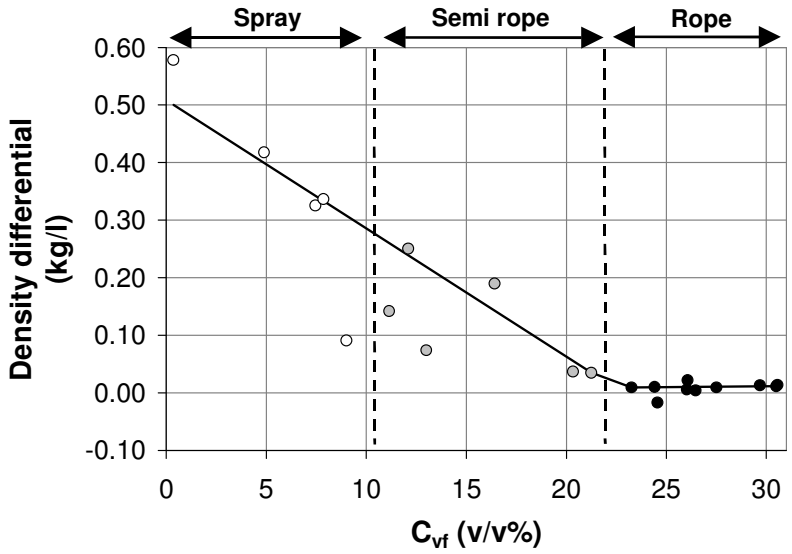

Figure 4.23. Density differential across the cyclone during the overloading of the 45mm spigot. Data points with white and grey backgrounds were obtained during spray and semi-rope discharges, respectively. While data points with black background were obtained during roping.

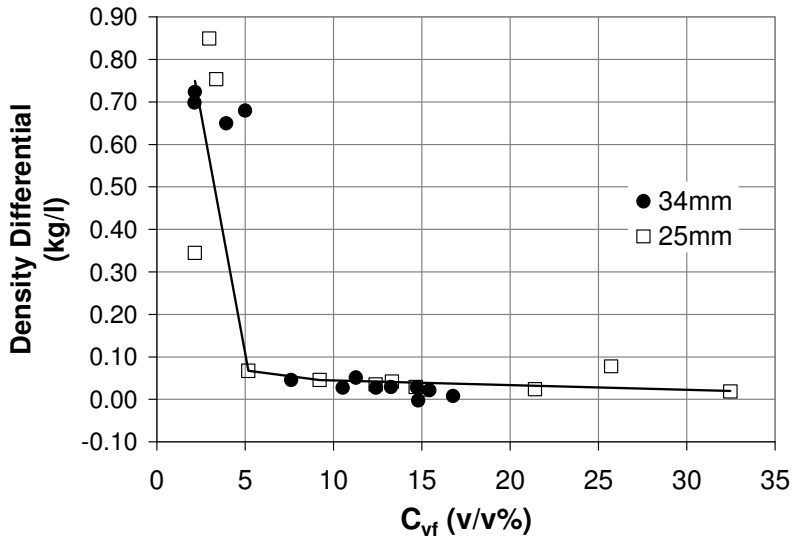

Figure 4.24. Density differential across the cyclone during the overloading of the 25 and 45mm spigots.

The range of density differentials obtained during all the tests performed with fine magnetite (95% -45µm) are shown in Fig. 4.25. This includes data from test-work aimed at determining the effect of various variables on the spigot capacity. The range of density differential obtained with medium and coarse grades ranged from –0.07 to 0.26 and 0.10 to 0.31, respectively.

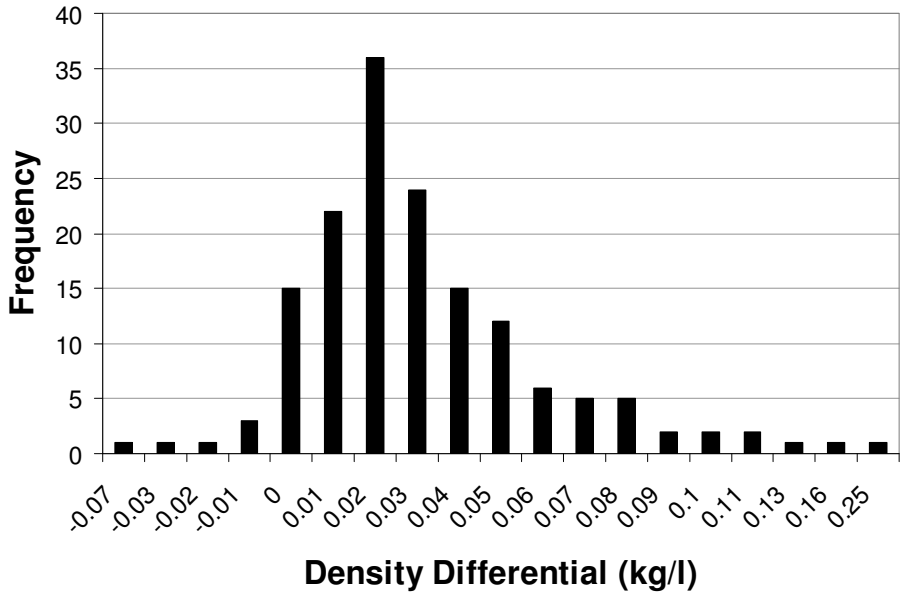

Figure 4.25. Range of density differential obtained during roping for all the tests performed with fine magnetite.

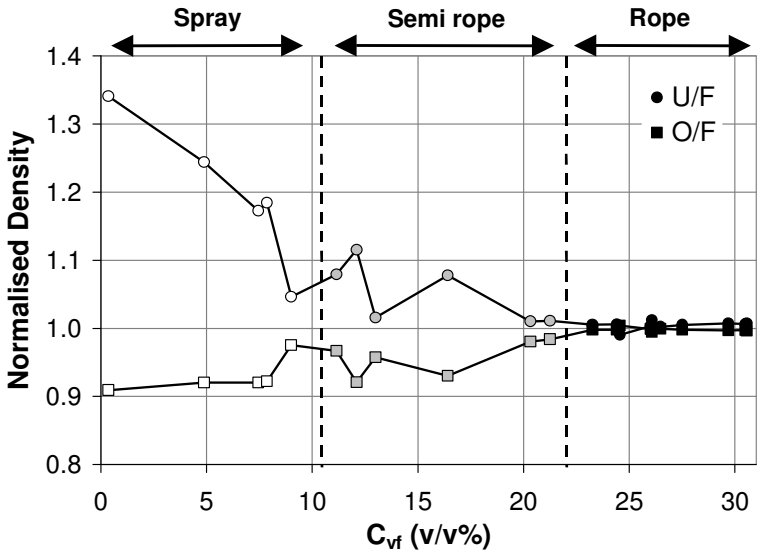

Figure 4.26. Influence of feed concentration on the floats and sinks medium densities for the 45mm spigot. Data points with white and grey backgrounds were obtained during spray and semi-rope discharges, respectively. While data points with black background were obtained during roping.

The floats and sinks medium densities were normalized to the feed density in Fig. 4.26, 4.27 and 4.28; the floats and sinks medium densities were increased and reduced, respectively, to equal the feed density during roping.

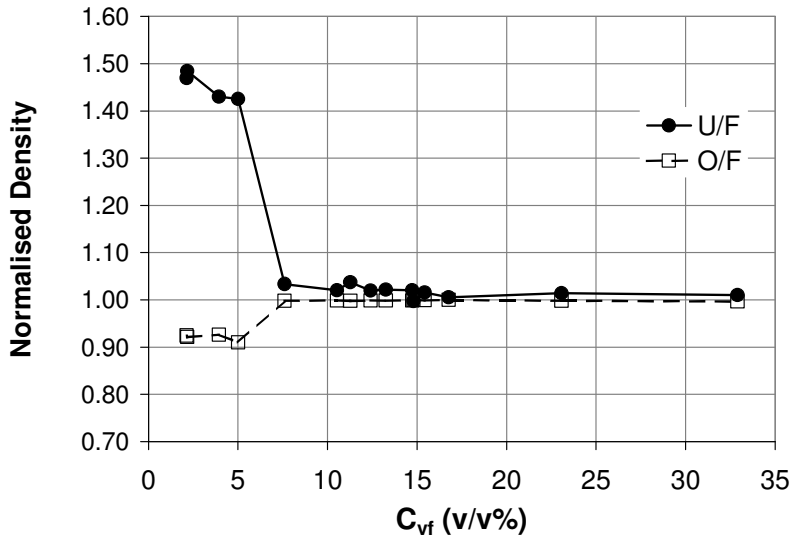

Figure 4.27. Influence of feed concentration on the floats and sinks medium densities for the 34mm spigot.

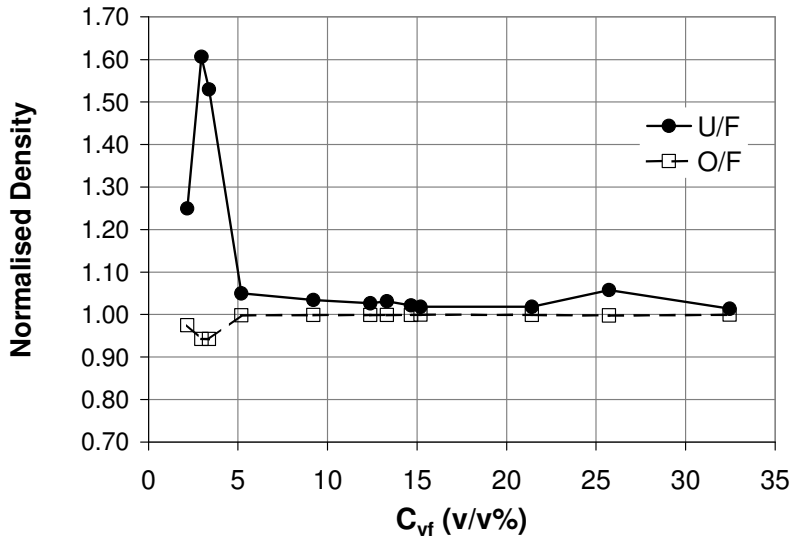

Figure 4.28. Influence of feed concentration on the floats and sinks medium densities for the 25mm spigot.

It is, therefore, expected that monitoring of the density differential could prove to be a useful diagnostic tool in detecting and avoiding spigot overloading in the cyclone.

4.2. QUANTIFYING THE SPIGOT CAPACITY

Jull (1972), Plitt et al. (1987), Heiskanen (2000) and DSM (1985) obtained mathematical expressions describing the relationship between spigot ore capacity and spigot diameter in accordance with the following relationship:

$$Q_{UM} = k_o D_u^{\ m} \qquad (2.13)$$

Heiskanen (2000) did not actually develop his own mathematical expression to quantify the spigot capacity, instead he validated Plitt et al. (1987)'s expression. The values for the constant k_o and exponent m for each of the relationships obtained by the various authors are shown in Table 2.21 (which is repeated here for convenience).

Table 2.21. Spigot diameter-spigot capacity relationships in literature.

Source	**Cyclone Type**	**Parameter** k_o	**Exponent** m
Jull (1972)	Classification	2.3	2.19
Plitt et al. (1987)	Classification	1.563	2.35
DSM (coal)	Dense medium	0.9	1.94
DSM (other minerals)	Dense medium	- *	2.05

*Dependent on head.

It, therefore, seems reasonable to expected Q_{USM} to be related to D_u in accordance with the following relationship:

$$Q_{USM} = kD_u^{\ n} \qquad (4.2)$$

Fitting equation 4.2 to all the data from the 165mm cyclone yielded the parameter values given in Table 4.3. The relationship between Q_{USM} and D_u is illustrated in Fig. 4.29; the plotted line in Fig. 4.29 represents equation 2.13, with the parameter values given in Table 4.3.

Table 4.3. Parameter values for equation 4.2 obtained for all the data acquired with the 165mm dense medium cyclone.

k	n	$\mathbf{R^2}$	$\boldsymbol{\sigma_{est}}$ **(l/hr slurry)**
21.97×10^{-3}	3.31	0.8088	1052.2

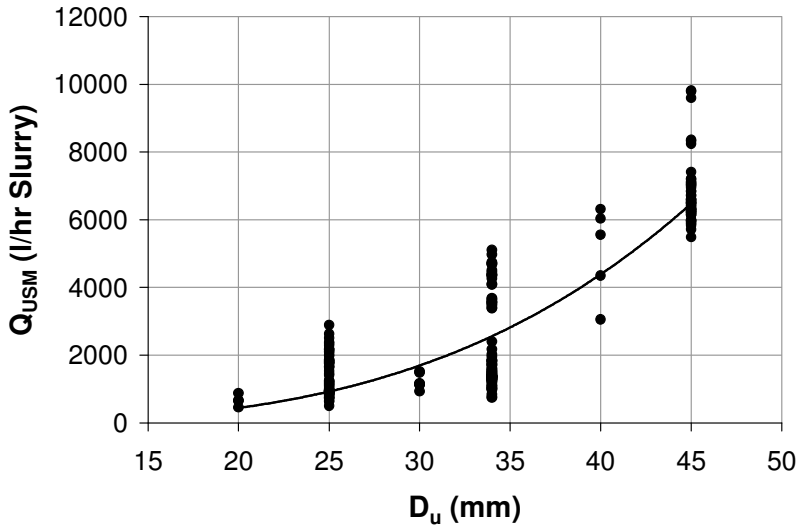

Figure 4.29. The effect of spigot diameter on Q_{USM}.

Fitting equation 2.13 to all the data from the 165mm cyclone yielded the parameter values presented in Table 4.4. The relationship between Q_{UM} and D_u is illustrated in Fig. 4.30; the plotted line represents equation 2.13 with the parameter values given in Table 4.4.

Table 4.4. Parameter values for equation 2.13 obtained for all the data acquired with the 165mm dense medium cyclone.

k_o	m	$\mathbf{R^2}$	$\boldsymbol{\sigma_{est}}$ **(l/hr ore)**
3.18×10^{-3}	3.64	0.8499	454.7

Fitting equations 2.13 and 4.2 to the 165mm cyclone data gave unsatisfactory results as illustrated in Tables 4.3 and 4.4, and Fig. 4.29 and 4.30. The exponent *n* and *m* obtained in both equations 2.13 and 4.2 are much higher than those reported in the literature (Table 2.21). Further, what appears to be an inflection point can be observed at the lower part of both Fig. 4.29 and 4.30, while none is apparent at the upper part of the curve. It was, therefore, decided to analyse the data obtained with the 15^o cone angle separately from those obtained with the 20^o cone angle.

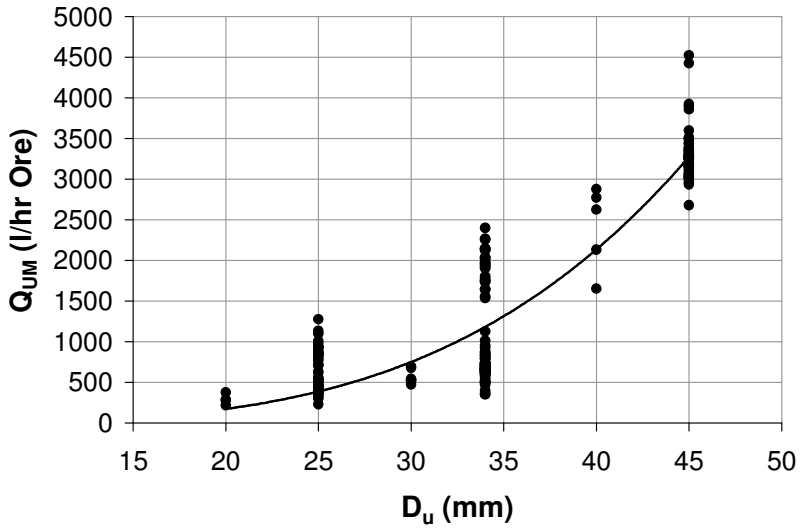

Figure 4.30. The effect of spigot diameter on Q_{UM}.

(a) 15^o Cone

The relationship between Q_{USM} and D_u for the 165mm cyclone when operating with a 15^o cone angle is shown in Fig. 4.31. An inflection point can clearly be observed at D_u is equal to 34mm. It appears that there was a change in 'flow regime' at the 34mm spigot diameter; beyond this spigot diameter Q_{USM} was more sensitive to changes in D_u. The relationship between Q_{UM} and D_u follows the same trend (Fig. 4.32).

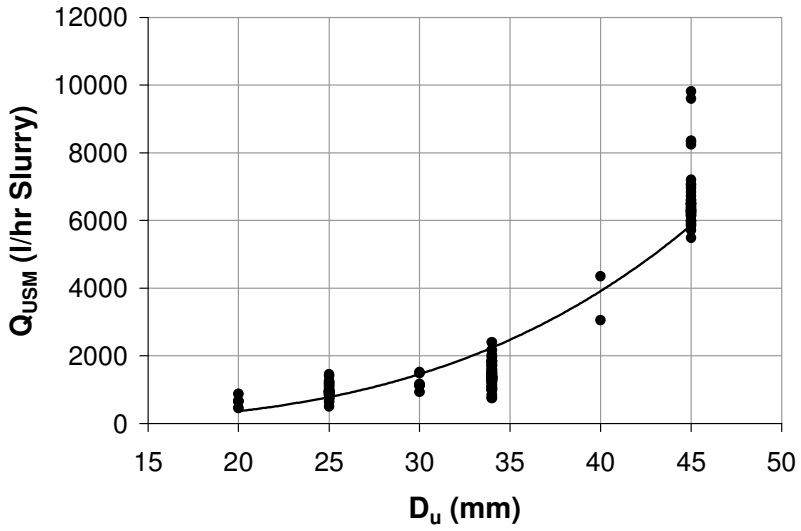

Figure 4.31. The effect of spigot diameter on Q_{USM} (15^o cone angle).

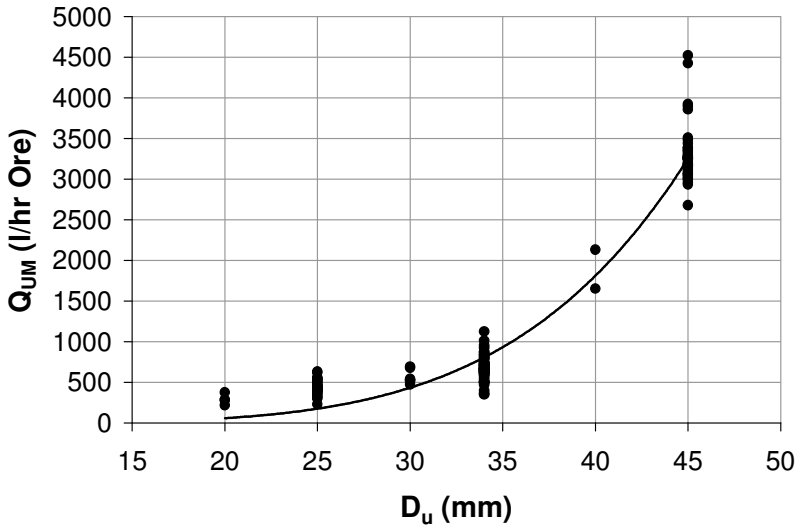

Figure 4.32. The effect of spigot diameter on Q_{UM} (15° cone angle).

Fitting equation 4.2 to all the data obtained with the 15° cone angle yielded the parameter values given in Table 4.5.

Table 4.5. Parameter values for equation 4.2 obtained for all the data acquired with the 165mm cyclone when operating with the 15° cone angle.

k	n	$\mathbf{R^2}$	$\boldsymbol{\sigma_{est}}$ **(l/hr slurry)**
12.63×10^{-3}	3.43	0.8747	895.2

Likewise fitting equation 2.13 to all the data obtained with the 15° cone angle yielded the parameter values given in Table 4.6. Analysis of the data obtained with the 15° cone angle separately from that obtained with the 20° one appears to have improved the quality of the fit, for both equation 2.13 and 4.2.

Table 4.6. Parameter values for equation 2.13 obtained for all the data acquired with the 165mm cyclone when operating with the 15° cone angle.

k_o	m	$\mathbf{R^2}$	$\boldsymbol{\sigma_{est}}$ **(l/hr ore)**
1.95×10^{-5}	4.98	0.9529	268.6

A schematic cross-section of the conical part of the cyclone for the 15° cone with the spigot inserted at the bottom is shown in Fig. 4.33. Fig. 4.33 (a) resembles the 45mm spigot, while the smaller spigots (20, 25, 30 and 34mm) look more like Fig. 4.33 (b). The 40mm spigot, on

the other hand, is in between the two configurations. The cone initially converges to a diameter of 45mm and then extends a length of about 225mm, of which the inserted spigot occupies only approximately 80mm. Thus, the slurry travels a distance of 145mm within 'cylindrical' part (with a diameter of 45mm) of the cone before reaching the inserted spigot. A consequence of this extra length is the accentuation of the effect of friction on the slurry flow at the sinks (increased resistance to flow), giving lower spigot capacities for the 15^o cone.

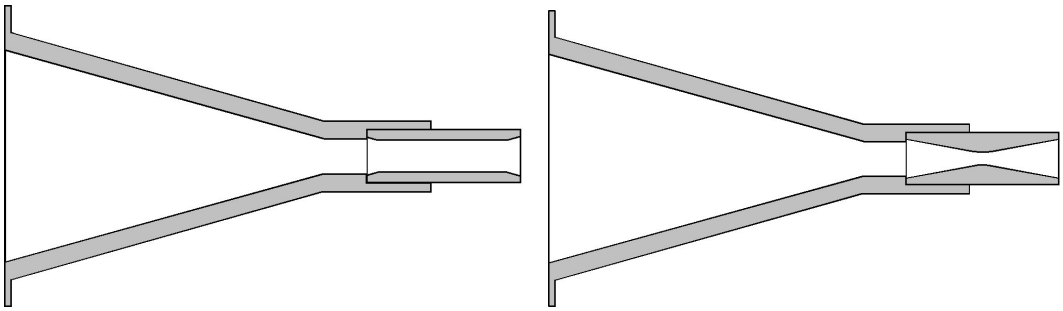

Figure 4.33. Schematic cross sectional view of the 15^o cone angle for (a) larger spigot and (b) smaller spigot.

It is interesting to note that the smaller spigots (20, 25, 30 and 34mm), which have a design resembling that in Fig. 4.33 (b), appear to be following one relationship, and the bigger spigots (40 and 45mm) appear to be following another. It is thought that the observed inflection point in Fig. 4.31 and 4.32 is a consequence of the above-mentioned differences in spigot design.

(b) 20^o Cone

The relationship between D_u and Q_{USM} for a cone angle of 20^o is shown in Fig. 4.34. The inflection point encountered with the 15^o cone was not observed with the 20^o cone. The same is true for the relationship between D_u and Q_{UM} (Fig. 4.35).

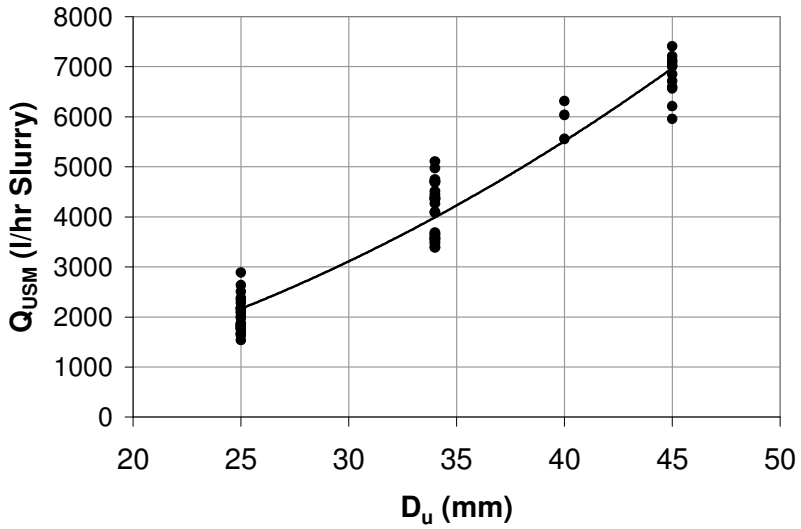

Figure 4.34. The effect of spigot diameter on Q_{USM}. (Cone A - 20°)

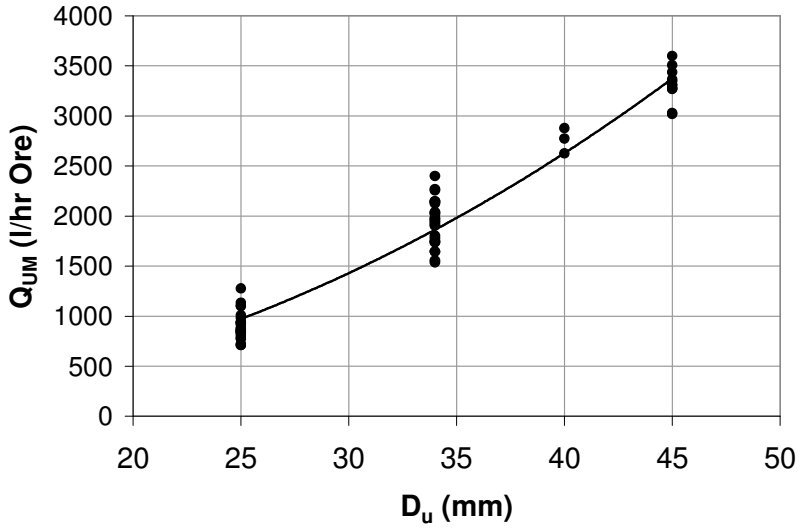

Figure 4.35. The effect of spigot diameter on Q_{UM}. (Cone A - 20°)

Fitting equation 4.2 to all the data obtained with the 20° cone angle yielded the parameter values given in Table 4.7. Likewise fitting equation 2.13 to all the data obtained with the 20° cone angle yielded the parameter values given in Table 4.8.

Table 4.7. Parameter values for equation 4.2 obtained for all the data acquired with the 165mm cyclone when operating with the 20° cone angle.

k	*n*	R^2	σ_{est} (l/hr slurry)
3.57	1.99	0.9361	468.6

Analysis of the data obtained with the 20° cone angle separately from those obtained with the 15° one clearly improved the quality of the fit for both equations 2.13 and 4.2 (Tables 4.7 and 4.8). Further the exponent *n* and *m* obtained in both equations 2.13 and 4.2, for the 20° cone angle, are in agreement with those reported in the literature (Table 2.21).

Table 4.8. Parameter values for equation 2.13 obtained for all the data acquired with the 165mm cyclone when operating with the 20° cone angle.

k_o	m	$\mathbf{R^2}$	$\boldsymbol{\sigma_{est}}$ **(l/hr ore)**
1.07	2.12	0.9548	194.6

A schematic cross-section of the conical part of the cyclone with the spigot inserted at the bottom of cone A is shown in Fig. 4.36. Just as with the 15° cone, Fig. 4.36 (a) resembles the 45mm spigot, while the smaller spigots (20, 25, 30 and 34mm) look more like Fig. 4.36 (b). Unlike the 15° cone, cone A converges down to a diameter of 50mm and the cone converges directly onto the inserted spigot. The extra length of about 145mm, present in the 15° cone-spigot design, was not present in this arrangement. It is thought that this might be the reason for the difference in the nature of the spigot diameter-spigot capacity relationships obtained between the 15° cone angle and cone A (20°).

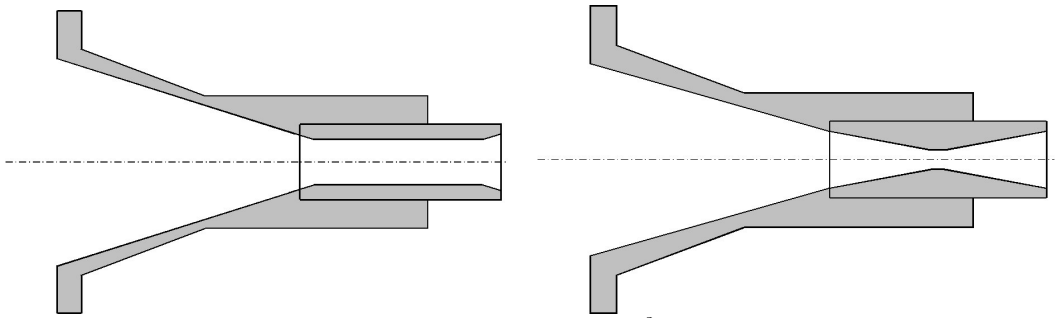

Figure 4.36. Schematic cross sectional view of cone A (20°) for (a) larger spigot and (b) smaller spigot.

In order to elucidate further the effect of the spigot design on the spigot capacities another 20° cone (cone B) with a different design from cone A was employed. Cone B differs from the cone A in that its spigot is not interchangeable; instead it is fixed at 45mm.

Figure 4.37. A picture of cone B.

A picture of cone B is shown in Fig. 4.37, and a schematic diagram of the cross-section through cone B is shown in Fig. 4.38.

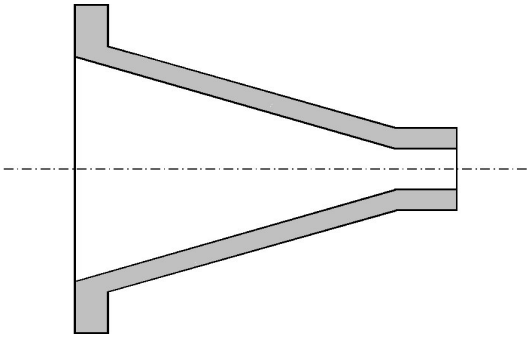

Figure 4.38. A schematic diagram of the cross-section through cone B.

A comparison between Q_{USM} values obtained with cone A and those with cone B is shown in Fig. 4.39. Q_{USM} values obtained with cone B were higher than those obtained with cone A. The differences in the Q_{USM} values were on average about 20%. The conditions under which the results given in Fig. 4.39 and 4.40 were obtained are presented in Table A.5 in Appendix A.

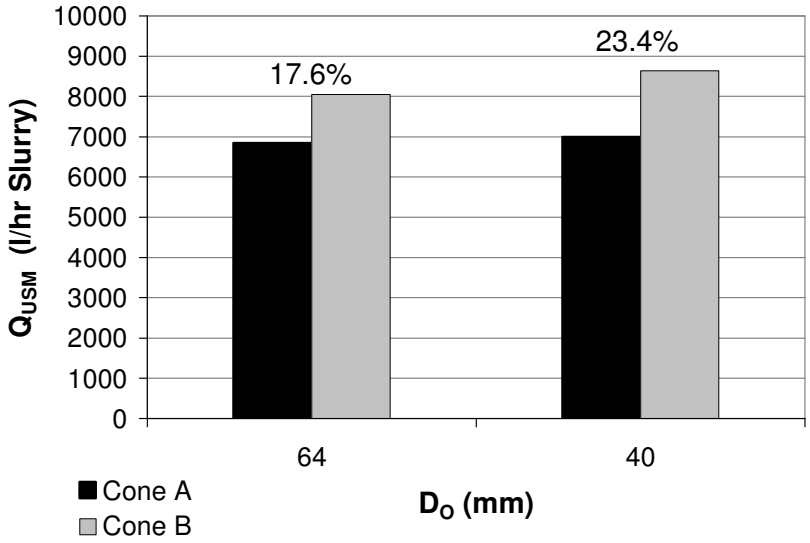

Figure 4.39. The influence of spigot design on Q_{USM}. (Operating conditions are given in Table A.5).

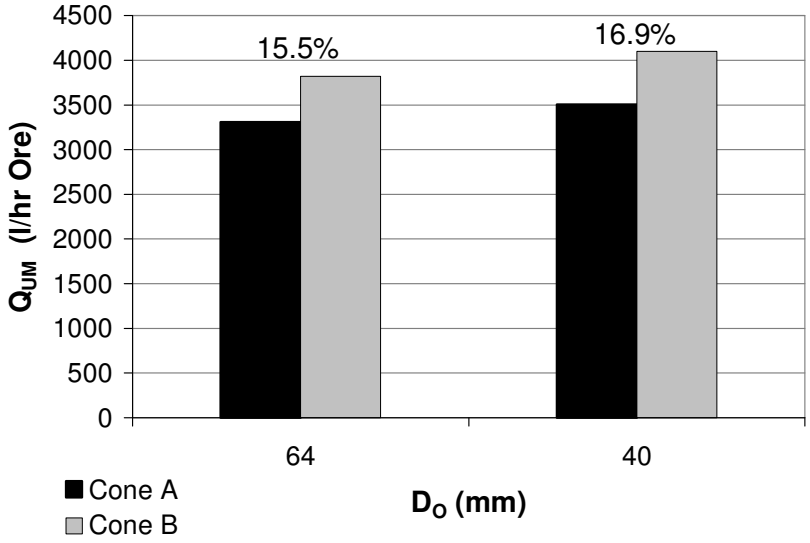

Figure 4.40. The influence of spigot design on Q_{UM}. (Operating conditions are given in Table A.5).

Similarly Q_{UM} values obtained with cone B were higher than those obtained with cone A by about 16% (Fig. 4.40). The main difference between cone A and B is that cone A (with the spigot inserted) is 115mm longer. It is this difference in length (at the sinks) that accounts for the lower spigot capacities obtained with cone A. These observations validate the postulation that the lower Q_{USM} and Q_{UM} values obtained with the 15^o cone angle were, at the least, partly due to the 145mm extra length present within the 15^o cone. It appears that the effect of this extra length is dependent on the size of the inserted spigot. The effect was more pronounced

at the smaller spigot diameters (34mm and less) at which the resistance to flow was the highest; hence, the presence of the inflection point.

It appears, therefore, that the DSM design gives the least resistance to flow; a typical DSM cyclone design is illustrated in Fig. 4.41.

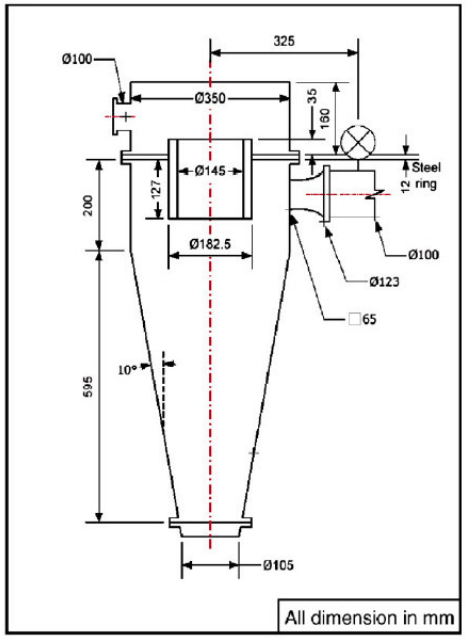

Figure 4.41. Configuration of a 350mm DSM cyclone. (Narasimha et al., 2007)

4.2.1. MODEL DEVELOPMENT

Empirical models quantifying/predicting various parameters including Q_{USM}, Q_{UM}, Q, S_R, C_{mvu} and R_m were developed making use of multiple-regression techniques. Only data obtained when operating the 165mm cyclone with cone A was utilized in developing the mathematical models that follow. None of the data obtained when operating with the 15^o cone angle was used in developing the models due to the presence of an inflection point as previously illustrated (Fig. 4.31 and 4.32). The behaviour encountered when operating with the 15^o cone angle is not well understood; hence, this data is left out in developing the regression models. The data acquired with the smaller 165mm cyclone (cone A only) were initially analysed separately, and then combined with those obtained with the larger 350mm cyclone. The dependent variables considered for the 165mm cyclone data include: Q_{USM}, Q_{UM}, Q, S_R, C_{mvu} and R_m. Only Q_{UM} was measured on the 350mm cyclone.

Multiple-regression procedure was repeated making use of different functional forms of the independent variables, namely: linear, power, exponential, etc. Only variables that were significant at the 95 percent confidence level were added to the regression equations. Although the spigot capacity is dependent mainly on D_u, it is expected that other variables should also have an effect on it. As a result a number of independent variables including D_o, D_i, Bl, H, ρ_{med}, and medium grade were considered.

(a) Spigot Capacity

The spigot capacity and spigot diameter have previously been illustrated in the literature to be correlated according to a power relationship, as in equation 2.12 and 2.13. Feed head has also been shown to correlate with the spigot capacity in accordance with a power relationship (Equation 2.12). Although mathematical correlations between D_o and D_i with spigot capacity have not previously been proposed, it seems reasonable to make use of a power relationship as with D_u and H. The relationship between spigot capacity and medium density appeared to be more complex than that of the other independent variables. Q_{USM} and Q_{UM} decreased with increasing ρ_{med}, and the sensitivity of both Q_{USM} and Q_{UM} to ρ_{med} increased beyond a certain critical value of ρ_{med}. In order to describe this behaviour the exponential term in equation 4.3 and 4.4 was employed. The best fit for both equation 4.3 and 4.4 was obtained when the critical ρ_{med} value was set at 1.45 kg/l; various ρ_{med} values ranging from 1.3 up to 1.7kg/l were attempted.

Hence, the following empirical model, which takes into account other variables other than D_u, to predict Q_{USM} is proposed:

$$Q_{USM} = kD_u^{n_1} D_o^{n_2} D_i^{n_3} H^{n_4} \exp\left[n_5(\rho_{med} - 1.45)^3\right] \quad (4.3)$$

with Q_{USM} in l/hr slurry, D_u in mm, D_o in mm, D_i in mm, H in D and ρ_{med} in kg/l. Fitting equation 4.3 to all the data obtained when operating the 165mm cyclone with cone A gave the parameter values given in Table 4.9. Medium grade and barrel length were found not to be significant at the 95 percent confidence level, and as a result they were left out of the regression equation. The P-value given in Table 4.9 is the probability of falsely rejecting the null hypothesis, or wrongfully concluding that there is an association between the dependent and independent variables.

Table 4.9. Summary of statistical results from multiple-regression of Q_{USM} data obtained with the 165mm cyclone (cone A).

	Coefficient	**Std Error**	**P-value**	**R^2**	**σ_{est} (l/hr slurry)**
k	0.394	0.156	0.0144	0.9805	267.3
n_1	2.09	0.046	<0.0001		
n_2	-0.14	0.045	0.0039		
n_3	0.43	0.070	<0.0001		
n_4	0.36	0.044	<0.0001		
n_5	-5.67	1.362	0.0001		

Equation 4.3 appears to predict Q_{USM} reasonably well. The goodness of fit is illustrated in Fig. 4.42 where the measured Q_{USM} values are compared with those predicted with equation 4.3.

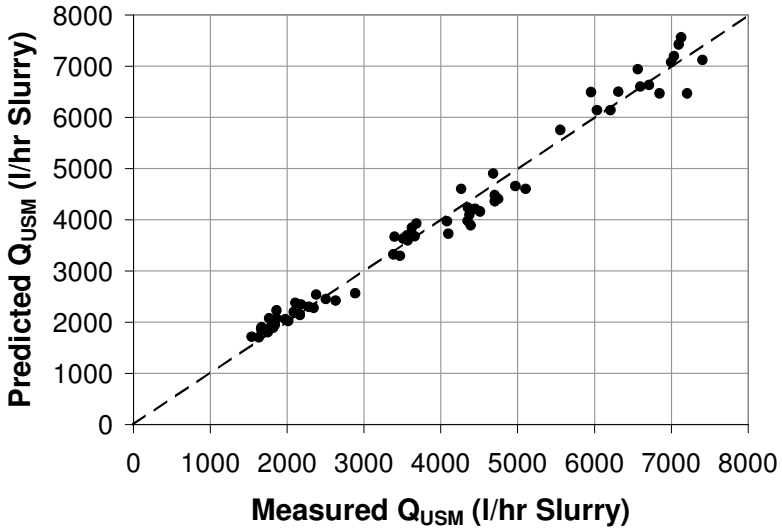

Figure 4.42. Predicted versus measured Q_{USM} values for equation 4.3 with parameter values in Table 4.9.

The following empirical model to predict Q_{UM} is proposed:

$$Q_{UM} = k_o D_u^{m_1} D_o^{m_2} D_i^{m_3} H^{m_4} \exp\left[m_5 (\rho_{med} - 1.45)^3\right] \quad (4.4)$$

with Q_{UM} in l/hr ore, D_u in mm, D_o in mm, D_i in mm, H in D and ρ_{med} in kg/l. Fitting equation 4.4 to all the data obtained when operating the 165mm cyclone with cone A gave the parameter values given in Table 4.10. Just as with Q_{USM}, medium grade and barrel length were found not to be significant at the 95 percent confidence level.

Table 4.10. Summary of statistical results from multiple-regression of Q_{UM} data obtained with the 165mm cyclone (cone A).

	Coefficient	**Std Error**	**P-value**	**R^2**	**σ_{est} (l/hr ore)**
k_o	0.226	0.091	0.0158	0.9821	126.7
m_1	2.16	0.046	<0.0001		
m_2	-0.11	0.046	0.0181		
m_3	0.38	0.072	<0.0001		
m_4	0.20	0.044	<0.0001		
m_5	-7.59	1.447	<0.0001		

Equation 4.4 appears to predict Q_{UM} reasonably well. The goodness of the fit is illustrated in Fig. 4.43, where the measured Q_{UM} values are compared with those predicted with equation 4.4.

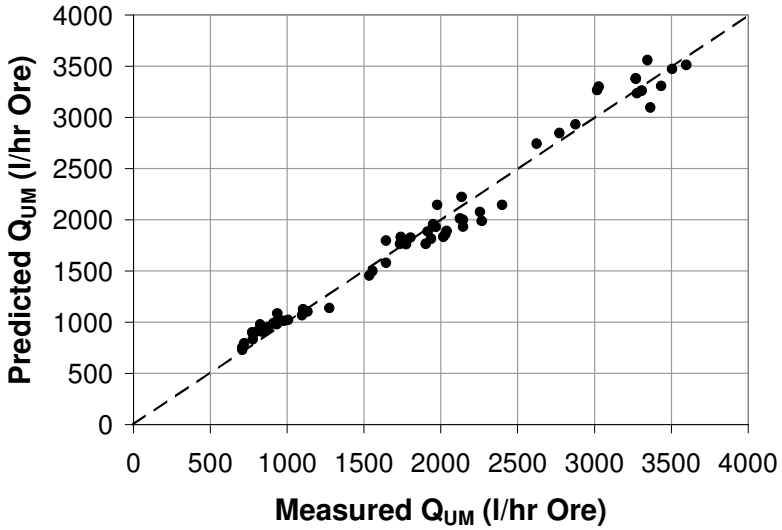

Figure 4.43. Predicted versus measured Q_{UM} values for equation 4.4 with parameter values in Table 4.10.

Inclusion of 350mm cyclone data

Data obtained with the 350mm cyclone showed Q_{UM} to reach a peak at a certain critical value of ρ_{med}, beyond which Q_{UM} decreased with further increases in ρ_{med}. In order to describe this 'peaking' behaviour the exponential term in equation 4.5 was employed; Fig. 4.44 illustrates how well this term describes the 'peaking' behaviour. The best fit for equation 4.5 was obtained when the critical ρ_{med} value was set at 1.45 kg/l just as was the case for equations 4.3 and 4.4; various ρ_{med} values ranging from 1.3 up to 1.7kg/l were attempted.

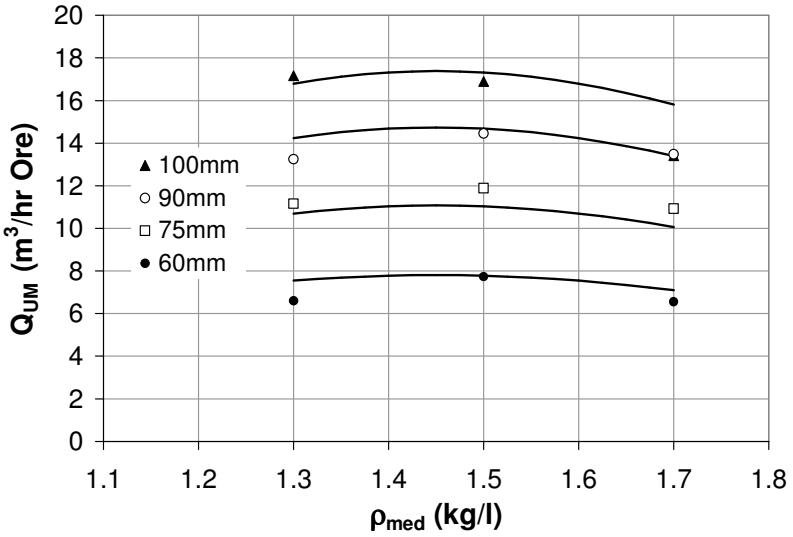

Figure 4.44. The effect of medium density on Q_{UM} for the 350mm cyclone. (The plotted lines represent equation 4.5.)

The following empirical model, which takes into account data from both the 165mm (cone A only) and 350mm cyclones, to predict Q_{UM} is proposed:

$$Q_{UM} = k_o D^{m_1} D_u^{m_2} H^{m_3} \exp\left[m_4 (\rho_{med} - 1.45)^2\right] \quad (4.5)$$

with Q_{UM} in l/hr ore, D_u in mm, D in mm, H in D and ρ_{med} in kg/l. The relevant parameter values for equation 4.5 are given in Table 4.11. It appears that Q_{UM} is less sensitive to changes in D_u for the 350mm cyclone; the exponent m_1 was reduced from 2.16 to 1.53. The exclusion of D_o and D_i from equation 4.5 is a consequence of the fact that these variables were not varied on the 350mm cyclone, rather than an indication of their influence on Q_{UM}.

Table 4.11. Summary of statistical results from multiple-regression of Q_{UM} data obtained with the 165mm (cone A) and 350mm cyclones.

	Coefficient	**Std Error**	**P-value**	**R^2**	**σ_{est} (l/hr ore)**
k_o	0.235	0.063	0.0003	0.991	440.0
m_1	0.63	0.045	<0.0001		
m_2	1.53	0.063	<0.0001		
m_3	0.18	0.063	0.0055		
m_4	-1.58	0.368	<0.0001		

An independent and significant effect of D on Q_{UM} is illustrated in Fig. 4.45. The dashed line in Fig. 4.45 represents Q_{UM} values that have been corrected for spigot design differences by increasing them by 20% (v/v). The figure of 20% is based on the results shown in Fig. 4.39 and 4.40, whereby the effect of spigot design on Q_{USM} and Q_{UM} was quantified. This correction does not entirely account for the differences in the spigot designs of the two cyclones. Although cone B is quite similar to the DSM design, it is not the same as illustrated in Fig. 4.38 and 4.41. Other factors that might possibly also contribute towards a discrepancy between results obtained with the 165mm and 350mm cyclones is their materials of construction and differences in inclination angle. The 165mm cyclone was constructed of polyurethane while the material of construction for the 350mm cyclone was cast iron. Although the afore-mentioned factors influence Q_{UM}, they do not account for the step increase in Q_{UM} values that is observed in Fig. 4.45 when the cyclone diameter is increased from 165mm to 350mm. It is thought that this is a consequence of the cyclone diameter; hence, it is included in equation 4.5.

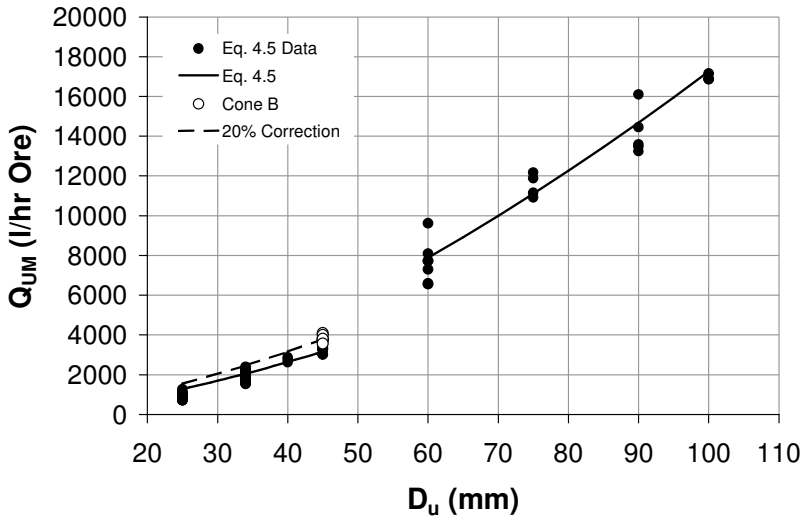

Figure 4.45. The effect of D_u on Q_{UM} for the 165mm and 350mm cyclones.

Equation 4.5 appears to predict Q_{UM} reasonably well. A comparison of the measured Q_{UM} values with those predicted with equation 4.5, for the data obtained with both the 165mm (cone A only) and 350mm cyclones, is shown in Fig. 4.46:

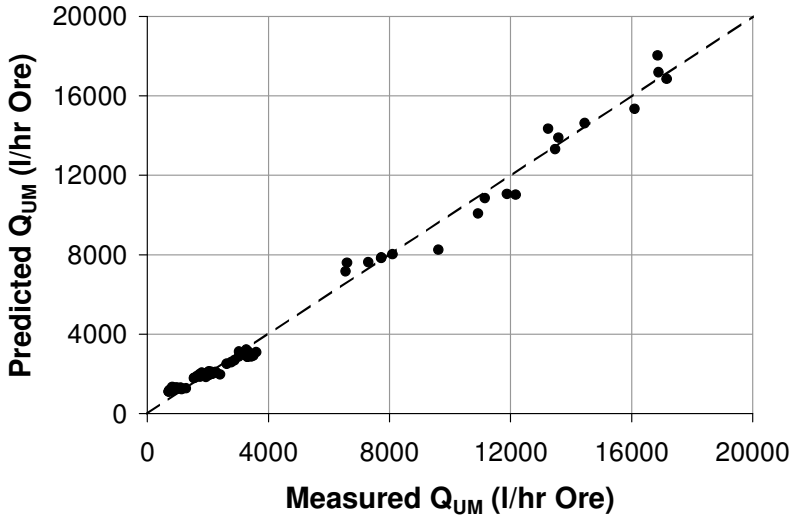

Figure 4.46. Predicted versus measured Q_{UM} values for equation 4.5 with parameter values in Table 4.11.

A closer look at Fig. 4.46 at the lower Q_{UM} values, which were obviously obtained with the 165mm cyclone, indicates that Q_{UM} was systematically over-estimated and under-estimated at the relatively lower and higher Q_{UM} values, respectively (Fig. 4.47). This is due to the differences in the sensitivity of Q_{UM} to D_u for the 165mm and 350mm cyclones.

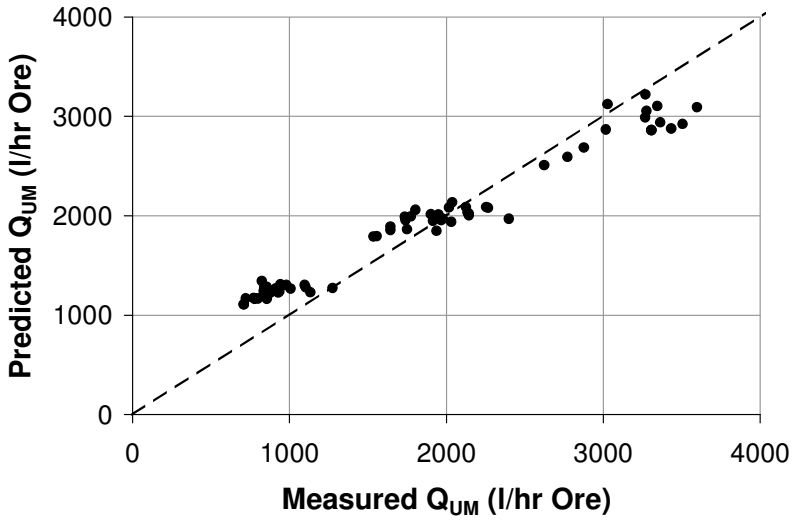

Figure 4.47. A closer look at the lower Q_{UM} values in Fig. 4.43.

(b) Cyclone Capacity

Upadrashta and Venkateswarlu (1982) proposed the following expression, which was determined during roping:

$$Q = K\left(\frac{P}{\rho_{med}}\right)^{0.58}(1-C_v)^{0.56}\left(D_u^2 + D_o^2\right)^{0.26} D_i^{1.8} \qquad \text{(A.2)}$$

Other expressions which were determined under spray discharge conditions are given in Appendix A (Equations A.1 to A.9). The use of the term $\left(D_u^2 + D_o^2\right)^n$ in equation 4.6 yielded the best fit; other functional forms yielded inferior correlations to that presented in Table 4.12. The increase in Q with increasing ρ_{med} is in contradiction with all other relationships reported in the literature. There is consensus in the literature that Q decreases with increasing ρ_{med}. The reasons for this contradiction are not clear.

Based on the expressions in the literature the following empirical model to predict Q seems reasonable:

$$Q = k\left(D_u + D_o\right)^{n_1} D_i^{n_2} H^{n_3} \rho_{med}^{n_4} \qquad \text{(4.6)}$$

with Q in l/hr slurry, D_o in mm, D_i in mm, H in D and ρ_{med} in kg/l. Fitting equation 4.6 to all the data obtained when operating the 165mm cyclone with cone A gave the parameter values given in Table 4.12. Only D_u, D_o, D_i, H and ρ_{med} were found to be significant at the 0.05 significance level.

Table 4.12. Summary of statistical results from multiple-regression of Q data obtained with the 165mm cyclone (cone A).

	Coefficient	Std Error	P-value	R^2	σ_{est} (l/hr slurry)
k	64.72	16.93	0.0003	0.9446	645.4
n_1	0.074	0.026	0.0057		
n_2	0.90	0.032	<0.0001		
n_3	0.62	0.034	<0.0001		
n_4	0.18	0.061	0.0052		

Equation 4.6 appears to give a fair prediction of Q. A comparison of Q values predicted with equation 4.6 and those measured is shown in Fig. 4.48.

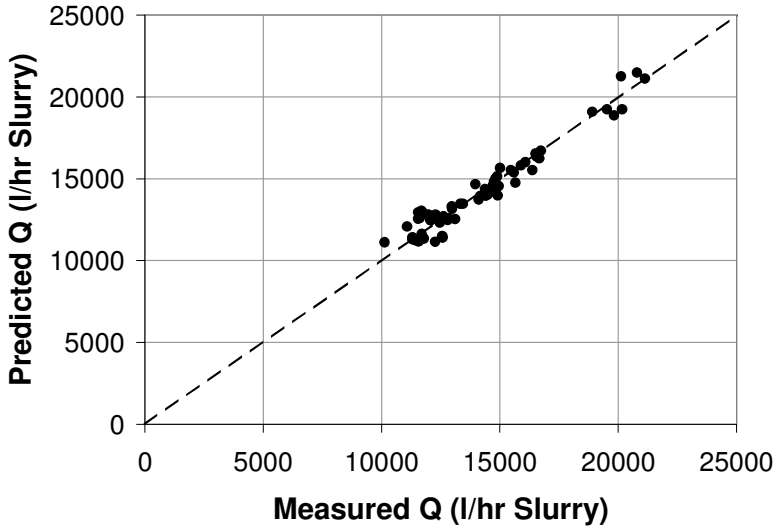

Figure 4.48. Predicted versus measured Q values for equation 4.6 with parameter values in Table 4.12.

(c) Volume Split

Upadrashta and Venkateswarlu (1982) proposed the following expressions, which was determined under roping conditions:

$$S_R = \frac{Q_{USM}}{Q_O} = 1.91(1-C_V)^{1.1} Q^{-0.44} \left(\frac{D_u}{D_o}\right)^{2.32} \qquad (2.9)$$

A combination of equations 2.9 and A.2 give the following expression:

$$S_R = \frac{Q_{USM}}{Q_O} \propto (1-C_V)^{0.85} \left(\frac{P}{\rho_{med}}\right)^{-0.26} \left(D_o^2 + D_u^2\right)^{-0.11} \left(\frac{D_u}{D_o}\right)^{2.32} D_i^{-0.79}$$

Usage of the following terms on the results obtained in this study did not yield an acceptable correlation:

$\left(D_o^2 + D_u^2\right)^{n_1}$ and $\left(\frac{D_u}{D_o}\right)^{n_2}$.

Instead a power relationship was employed to correlate S_R with D_o and D_u. Misplacement of sinks particles to the floats stream did not influence S_R in the same way in the current study as reported by Upadrashta and Venkateswarlu (1982). S_R increased with increasing C_{vf} in the current investigation while Upadrashta and Venkateswarlu reported it to decrease with increasing C_V. A power relationship was used to correlate H with S_R and this gave reasonable results.

The following empirical model to predict S_R is, therefore, proposed:

$$S_R = \frac{Q_{USM}}{Q_{OS}} = 10^k D_u^{n_1} D_o^{n_2} H^{n_3} C_{vf}^{n_4} \qquad (4.7)$$

with Q_{USM} in l/hr slurry, Q_{OS} in l/hr slurry, D_u in mm, D_o in mm, H in D and C_{vf} in %v/v. Fitting equation 4.7 to all the data obtained when operating the 165mm cyclone with cone A gave the parameter values given in Table 4.13. Only D_u, D_o, H and C_{vf} were found to be significant at the 0.05 significance level.

Table 4.13. Summary of statistical results from multiple-regression of data obtained with the 165mm cyclone (cone A).

	Coefficient	**Std Error**	**P-value**	**R^2**	**σ_{est} (v/v)**
k	-4.52	0.3145	<0.0001	0.9637	0.081
n_1	2.76	0.1816	<0.0001		
n_2	-0.25	0.0904	0.0071		
n_3	-0.70	0.0983	<0.0001		
n_4	0.83	0.1564	<0.0001		

Equation 4.7 appears to give a fair prediction of S_R. A comparison of the measured S_R values with those predicted with equation 4.7 is shown in Fig. 4.49.

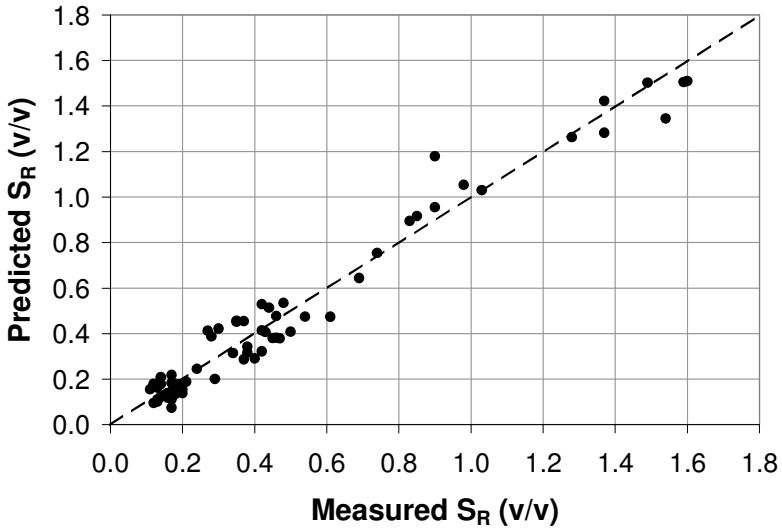

Figure 4.49. Predicted versus measured S values for equation 4.7 with parameter values in Table 4.13.

(d) Sinks Ore Concentration

C_{mvu} was found to be dependent on other independent variables as illustrated in equation 4.8:

$$C_{mvu} = kD_u^{a_1} Gr^{a_2} \qquad (4.8)$$

with C_{mvu} in %v/v, D_u in mm and Gr in mass percentage passing 45µm. Only D_u and medium grade were found to be significant at the 95 percent confidence level, and the correlation was poor (Table 4.14). Parameter values obtained from fitting equation 4.8 to all the data obtained with the 165mm cyclone operating with cone A are given in Table 4.14.

Table 4.14. Summary of statistical results from multiple-regression of C_{mvu} data obtained with the 165mm cyclone (cone A).

	Coefficient	**Std Error**	**P-value**	**R^2**	**σ_{est} (v/v%)**
k	139.34	44.65	0.0028	0.6702	1.38
a_1	0.14	0.017	<0.0001		
a_2	-0.35	0.073	<0.0001		

A comparison of the C_{mvu} calculated with equation 4.8 and those measured during experimental work is shown in Fig. 4.50. The quality of fit is illustrated to be very poor; this correlation is, therefore, of no significance.

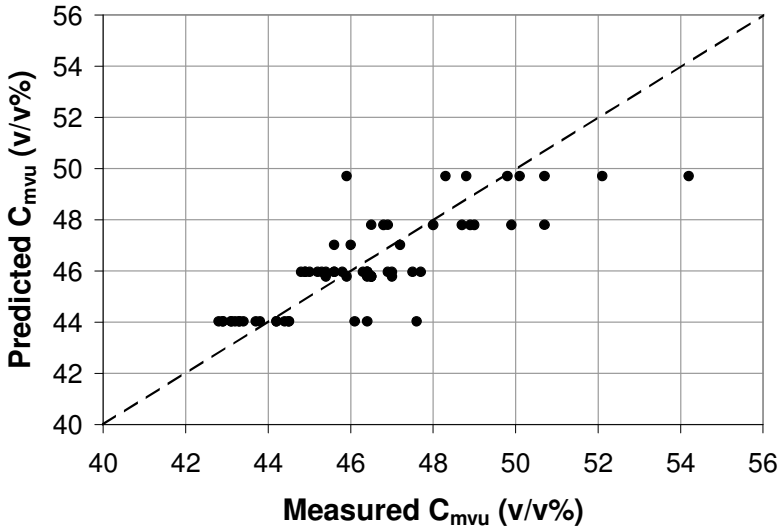

Figure 4.50. Predicted versus measured C_{mvu} values for equation 4.8 with parameter values in Table 4.14.

(e) Medium Split to Sinks

Clarkson and Wood (1993) proposed the following relationship, which was determined with a cyclone operating with medium only:

$$R_m = 0.79\left(\frac{D_u}{D_o}\right)^{4.2} H^{-0.37} \qquad (4.9)$$

Davis and Napier-Munn (1987), on the other hand, reported R_m to be a function of spigot diameter and kinematic viscosity. D_o and D_u were observed not to influence R_m as a ratio in the current study. Further, C_{vf} was observed to influence R_m significantly in the current investigation.

R_m was found to be dependent on other independent variables as illustrated in equation 4.10:

$$R_m = 10^k D_u^{b_1} D_o^{b_2} H^{b_3} C_{vf}^{b_4} \qquad (4.10)$$

with R_m in v/v, D_u in mm, D_o in mm, H in D and C_{vf} in v/v%. D_i, ρ_{med} and medium grade were found not to be significant at the 95 percent confidence level. Fitting equation 4.10 to all the data obtained when operating the 165mm cyclone with cone A gave the parameter values given in Table 4.15.

Table 4.15. Summary of statistical results from multiple-regression of R_m data obtained with the 165mm cyclone (cone A).

	Coefficient	**Std Error**	**P-value**	**R^2**	**σ_{est} (v/v)**
k	-3.78	0.2255	<0.0001	0.9600	0.024
b_1	1.96	0.1104	<0.0001		
b_2	-0.25	0.0716	0.0009		
b_3	-0.17	0.0746	0.0247		
b_4	0.52	0.0983	<0.0001		

Equation 4.9 appears to give a fair prediction of R_m. A comparison of the measured R_m values with those predicted with equation 4.10 is shown in Fig. 4.51.

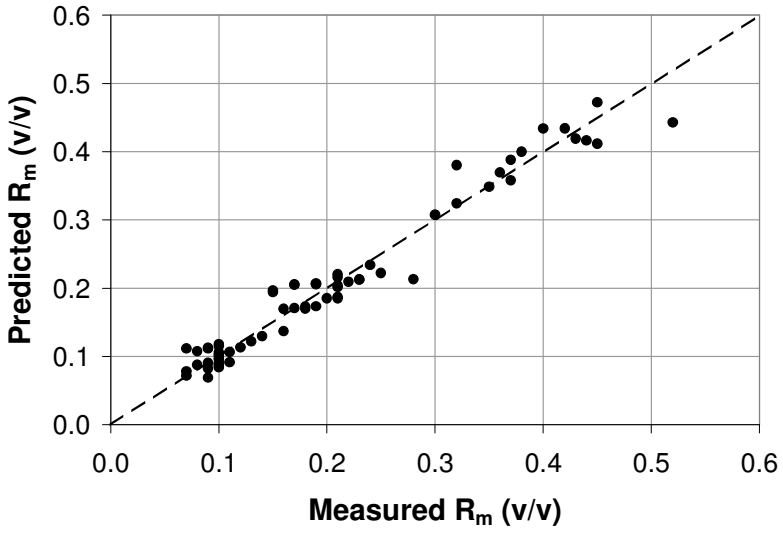

Figure 4.51. Predicted versus measured R_m values for equation 4.10 with parameter values in Table 4.15.

4.2.2. Comparison with DSM Spigot Capacities

A comparison between the spigot ore capacities obtained in this study with those by DSM is shown in Fig. 4.52 and 4.53; a log-log scale is used in Fig. 4.56 for clarity especially at the smaller spigot diameters. The spigot capacities obtained in this study are consistently higher than those by DSM.

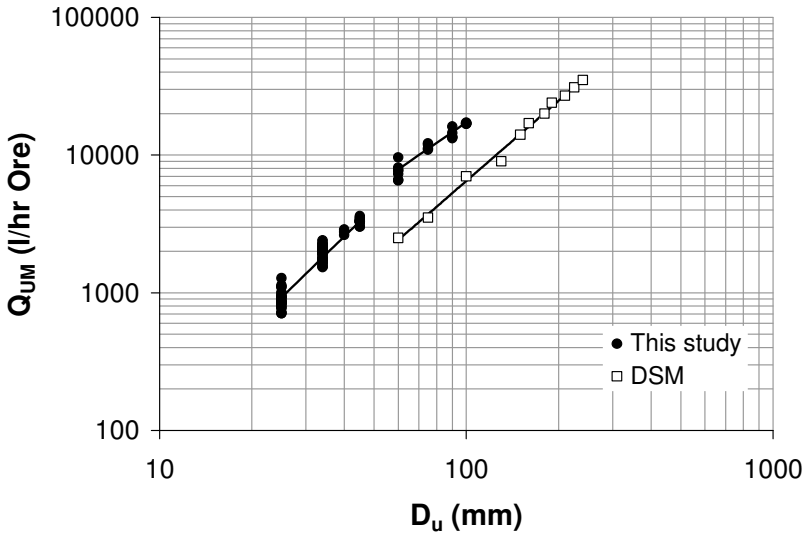

Figure 4.52. Comparison of the spigot diameter-spigot capacity relationship obtained in this study with that by DSM.

The differences between Q_{UM} values obtained in this investigation and those by DSM are quantified in Fig. 4.53 and Table 4.16 for D_u ranging from 60 to 100mm. Q_{UM} values obtained in this study were generally more than double those specified by DSM; a safety factor of around 60% was established. It can, therefore, be concluded that there is large potential to increase the 'spigot capacities' specified by DSM. In support of this view, Wood (1990) previously reported a case in which the volumetric sinks medium-to-ore ratio of a dense medium cyclone was 0.9:1 (53% ore by volume) and no serious symptoms such as gross misplacement of sinks particles to floats stream was observed. Further, he reported that only a 'little disruption to efficient separation' was encountered.

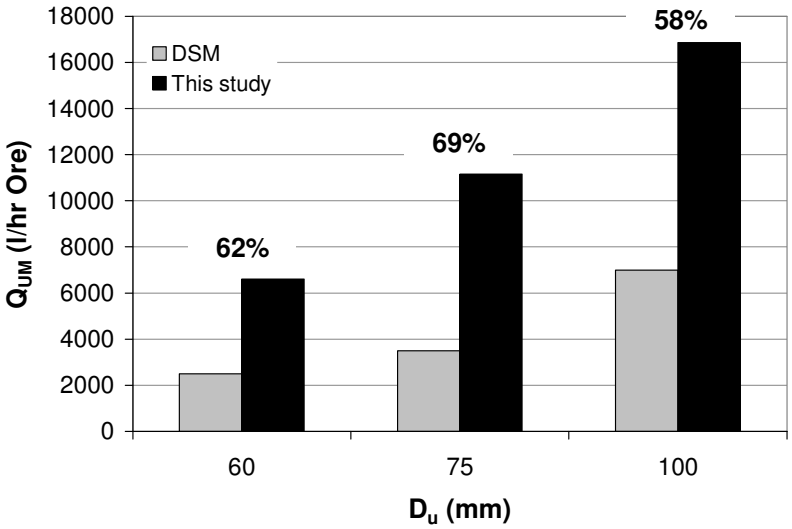

Figure 4.53. Comparison of Q_{UM} obtained in this study and those specified by DSM.

Table 4.16. Comparison of Q_{UM} obtained in this study and those specified by DSM.

D_u (mm)	Q_{UM} (l/hr ore)		
	This study	DSM	Safety Factor
60	6599	2500	0.62
75	11154	3500	0.69
100	16860	7000	0.58

Safety Factor = $(Q_{UM(This\ study)} - Q_{UM(DSM)})/Q_{UM(This\ study)}$

It is interesting to note that the spigot loading (in l/hr ore) at the transition point from a spray to semi-rope discharge is about 40% of the maximum spigot capacity (as shown Fig. 4.4, which is repeated here for convenience), so that the relevant safety factor is as follows:

$$\text{Safety factor} \approx \frac{3200-1350}{3200} = 58\%$$

This value is consistent with the values given in Table 4.16 and Fig. 4.53; implying that DSM possibly defined their 'spigot capacities' as the maximum spigot loading that can be achieved before semi-roping commences. This notion is further supported by the sinks ore concentrations (at the DSM specified 'spigot capacities'), which were inferred from the DSM data; these concentrations largely ranged between 24 and 31% (v/v) as given previously in Table 2.7. As previously mentioned, spigot overloading (or roping) is expected at sinks ore concentrations of 40% (v/v) and above, and semi-roping precedes rope discharge. Thus, the

sinks ore concentrations inferred from the DSM data are consistent with semi-roping conditions.

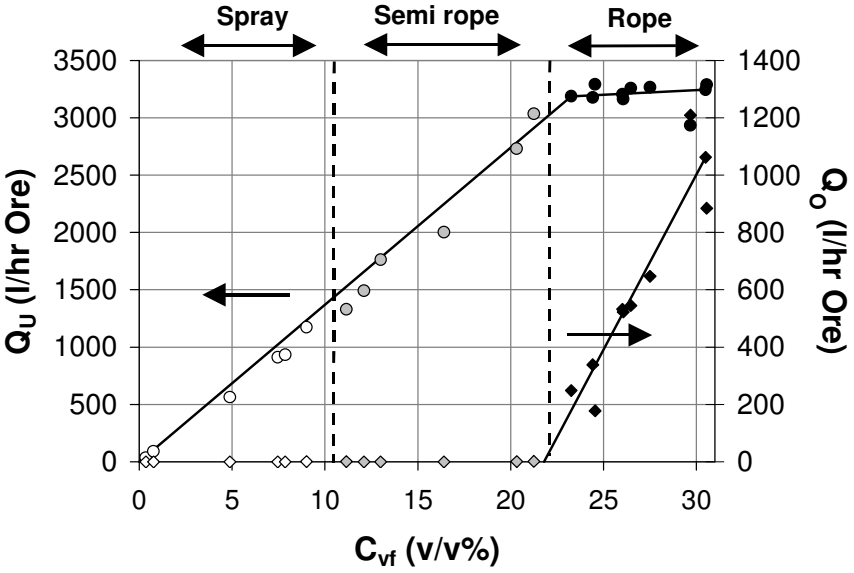

Figure 4.4. Changes in the ore loading at both the floats and sinks streams as ore was added into the cyclone for a 45mm spigot. Data points with white and grey backgrounds were obtained during spray and semi-rope discharges, respectively. While data points with black background were obtained during roping.

The DSM data presented in Fig. 4.52 and 4.53 was determined on geometrically similar cyclones, whilst that was not the case in this study. As previously illustrated, cyclone diameter has an independent and significant influence on Q_{UM}, and the data presented in Fig. 4.52 and 4.53 has not been corrected for this effect. In an attempt to correct this effect of cyclone diameter, equation 4.5 was utilized to predict Q_{UM} values of cyclones with diameters 165, 200, 250 and 350 with standard spigot sizes (D_u/D =0.3). The feed head was kept at 10D and the medium density at 1.5kg/l. The results of this exercise are given in Table 4.17 and Fig. 4.54. This correction gives a slightly lower safety factor of about 55% (Table 4.17).

Table 4.17. Comparison of Q_{UM} predicted with eq. 4.5 and those specified by DSM.

D (mm)	D_u (mm)	Q_{UM} (l/hr ore)		
		Eq. 4.5	DSM	Safety Factor
165	45	3016	–	–
200	60	5290	2500	0.53
250	75	8570	3500	0.59
350	100	16461	7000	0.57

Regression of the data (predicted with eq. 4.5) in Fig. 4.54 gave the following expression:

$$Q_{UM} = 0.642 D_u^{2.20} \quad (R^2 = 0.9997) \qquad (4.11)$$

with Q_{UM} in l/hr ore and D_u in mm. This expression describes the spigot ore capacities of geometrically similar cyclones at specific operating conditions, in this case being at a head of 10D and medium density of 1.5kg/l.

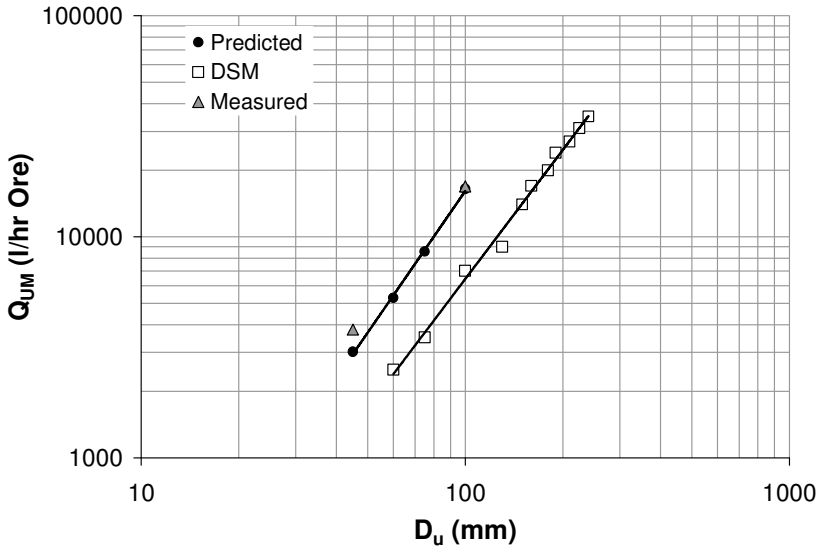

Figure 4.54. Comparison of Q_{UM} predicted from eq. 4.5 (to correct for effect of D) and those specified by DSM.

Assuming that this safety factor of about 50% determined in Table 4.17 holds for all conditions, then the spigot ore capacities for the larger cyclones would be as given in Fig. 4.55. The extrapolated spigot ore capacities in Fig. 4.55 are at best estimates; experimental work is required to valid them.

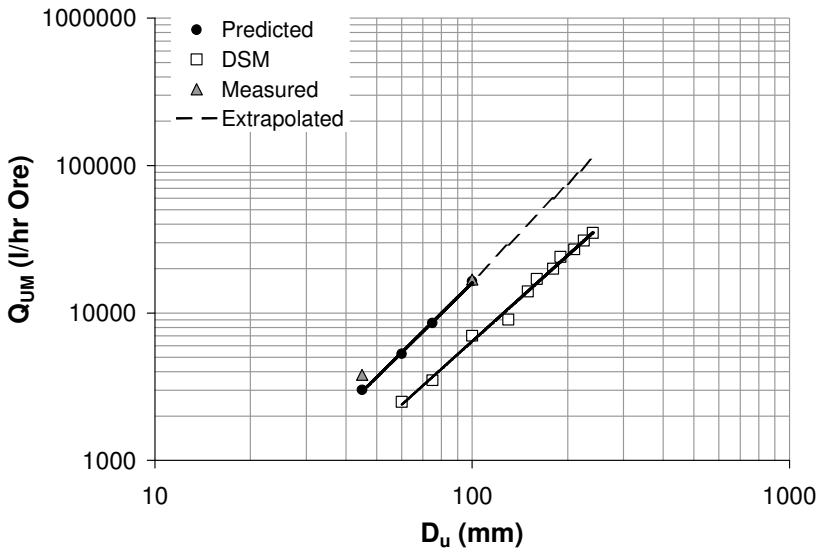

Figure 4.55. Comparison of Q_{UM} predicted from eq. 4.5 (to correct for effect of D) and those specified by DSM. Dashed line is extrapolation of eq. 4.11.

4.2.3. Influence of Cyclone Geometry on Spigot Capacity

(a) Spigot Diameter

As expected D_u was found to be the variable that influenced Q_{USM} the most; the relationship found was of the following form:

$$Q_{USM} \propto D_u^{2.09} \quad \text{(Eq. 4.3)}$$

Q_{UM} was also correlated to D_u in a similar manner:

$$Q_{UM} \propto D_u^{2.16} \quad \text{(Eq. 4.4)}$$

$$Q_{UM} \propto D_u^{1.53} \quad \text{(Eq. 4.5)}$$

The nature of the relationship between Q_{UM} and Q_{USM}, and D_u, especially for the data obtained with the 165mm cyclone operating with the cone A, is in agreement with the literature. Jull (1972) and Plitt et al. (1987) obtained the exponent for the Q_{UM}-D_u relationship to be 2.12 and 2.35, respectively. While DSM obtained the exponent to be 1.94 and 2.05 for coal and other minerals (not being coal), respectively. Q_{UM} was, however, less sensitive to changes in D_u for the relationship that included data from both the 165mm and 350mm cyclones.

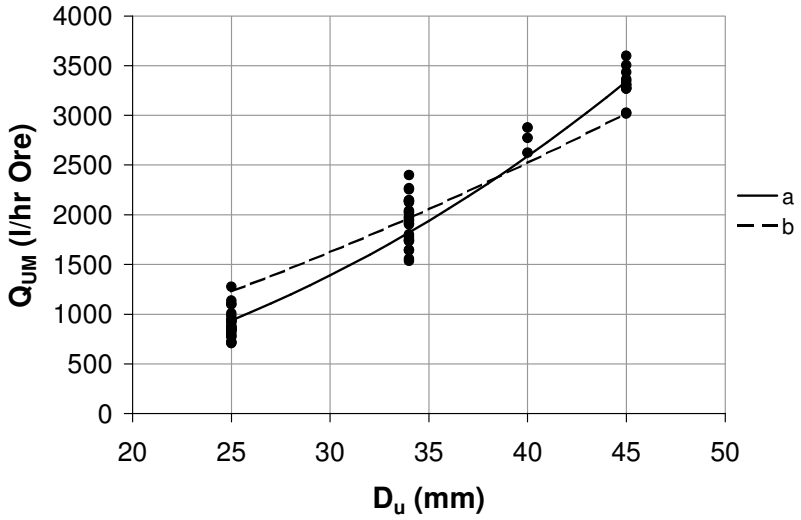

Figure 4.56. The effect of D_u on Q_{UM} for the 165mm cyclone operating with cone A. Plotted lines represent **a.** equation 4.4, and **b**. equation 4.5.

Although Q_{UM} was less sensitive to D_u for the larger 350mm cyclone, D_u still remained the most influential of all the variables tested. The effect of D_u on Q_{UM} is shown in Fig. 4.56 and 4.50. A comparison of equation 4.4 and 4.5 on the data obtained with the 165mm cyclone (cone A only) is shown in Fig. 4.56. The model based on the 165mm cyclone describes this data (shown in Fig. 4.56) much better than that based on both cyclones. The latter does, however, describe the data obtained with the larger 350mm cyclone reasonably well. This is illustrated in Fig. 4.57.

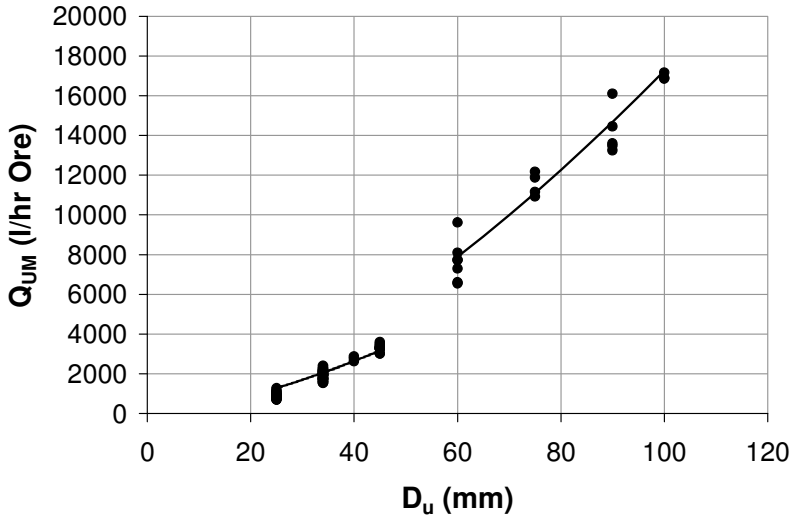

Figure 4.57. The effect of D_u on Q_{UM} for both the 165mm (cone A) and 350mm cyclones. Plotted lines represent equations 4.4 ($D_u \leq 45$mm) and 4.5 ($D_u \geq 60$mm).

The change in the sensitivity of Q_{UM} to D_u at larger cyclone diameters was also reported by Jull (1972), and Mular and Jull (1978) as illustrated in Fig. 4.58. Just as in the current study, Jull (1972) also observed Q_{UM} to be more sensitive to D_u at the smaller spigot sizes. According to Jull (1972) the spigot capacities of smaller cyclones are dependent on the cyclone geometry and certain operating conditions; hence, a range of spigot capacities is given for smaller cyclones in Fig. 4.58.

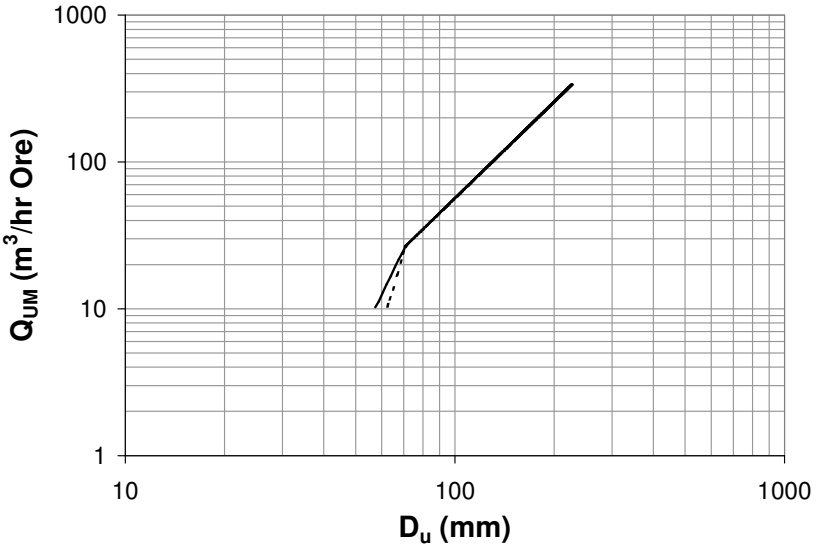

Figure 4.58. The effect of D_u on Q_{UM}. (Jull, 1972)

As previously illustrated, C_{mvu} is an important parameter that determines the onset of roping. It was found to be poorly related to D_u in the following manner:

$$C_{mvu} \propto D_u^{0.14}$$

C_{mvu} increased slightly with increasing D_u; this effect is illustrated in Fig. 4.59. An increase in C_{mvu} means that roping will take place at high ore concentrations at the sinks. This behaviour is in agreement with the literature; a similar trend has also been reported by Fahlstrom (1963) and Heiskanen (2000).

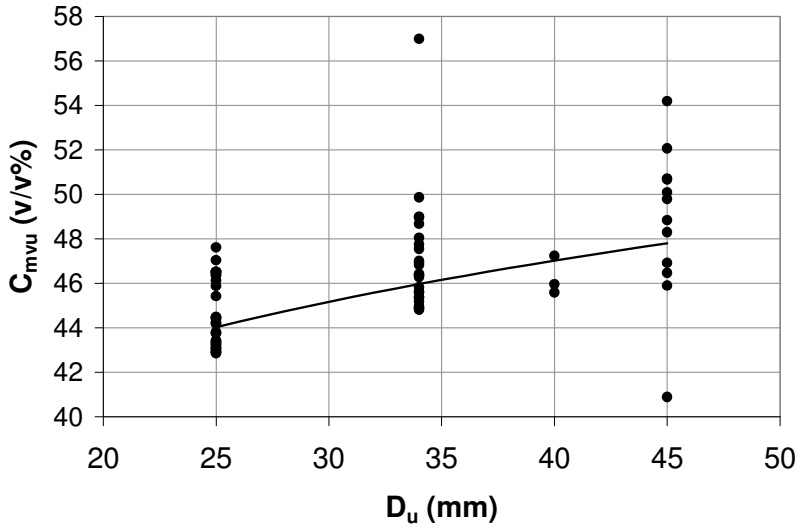

Figure 4.59. The effect of D_u on C_{mvu}. (Cone A - 20°)

Fig. 4.60 shows the change in the porosity of packed beds of various solids in tubes as the ratio of the particle diameter to the vessel diameter is increased. An increase in the particle diameter-to-vessel diameter ratio increases the porosity of packed solid particles, and consequently decreases their packing densities. At the extreme condition when the particle diameter-to-vessel diameter ratio approaches unity, for solids with a very narrow size distribution, the particles arrangement within the vessel would be such that very few particles can be accommodated in a single plane perpendicular to the length of the tube. In such a scenario excessive porosity will be observed, and very low packing densities will be achieved. The porosity of the solids under these conditions is determined not only by the particles' dimensions but also by the effect of the vessel/tube wall, which tends to push the particle inward and, consequently, create more voids closer to the walls. When the particle diameter-to-vessel diameter ratio approaches zero the porosity of the particles would be determined by the dimensions of the particles only, and the effect of the tube wall would be negligible. Thus, under these conditions the highest packing density of solids will be achieved.

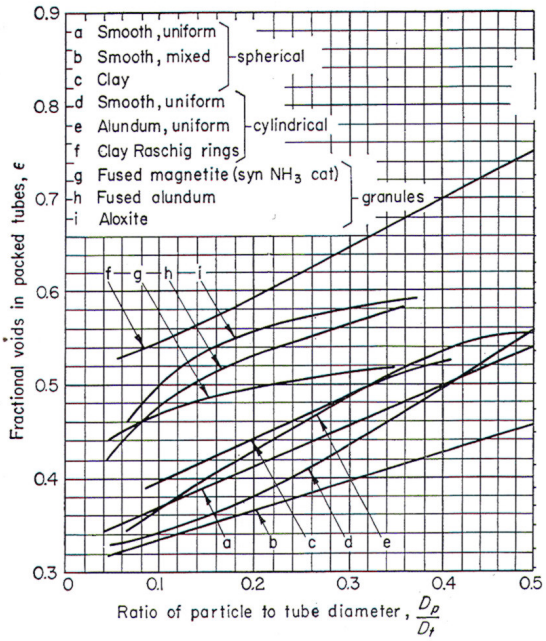

Figure 4.60. Porosity in tubes packed with various materials for increasing ratios of particle diameter to tube diameter. (Leva, 1959)

It is thought that the effect of spigot diameter on the sinks ore concentration is according to the above-mentioned behaviour. Although, strictly speaking, the arrangement of solids at the sinks during roping does not necessarily represent a packed bed, it is expected that the above-mentioned behaviour should be applicable to the conditions in the current investigation.

Particles referred to in Fig. 4.60 ranged from 2.5-18.5mm in size, while the tube diameters were 15.2-101.6mm.

R_m increased with increasing D_u as illustrated in Fig. 4.61. The relationship between R_m and D_u was of the following form:

$$R_m \propto D_u^{1.96}$$

The effect of D_u on R_m appears to be in accordance to D_u's influence on Q_{USM}. Further, the sensitivity of R_m to D_u observed in the current study is much less than that reported by Clarkson and Wood (1993), and Napier-Munn (1987) who reported the exponent to be 4.2 and 4.8, respectively. It is, however, worth noting that both Clarkson and Wood (1993), and Napier-Munn (1987) operated their cyclones with medium only.

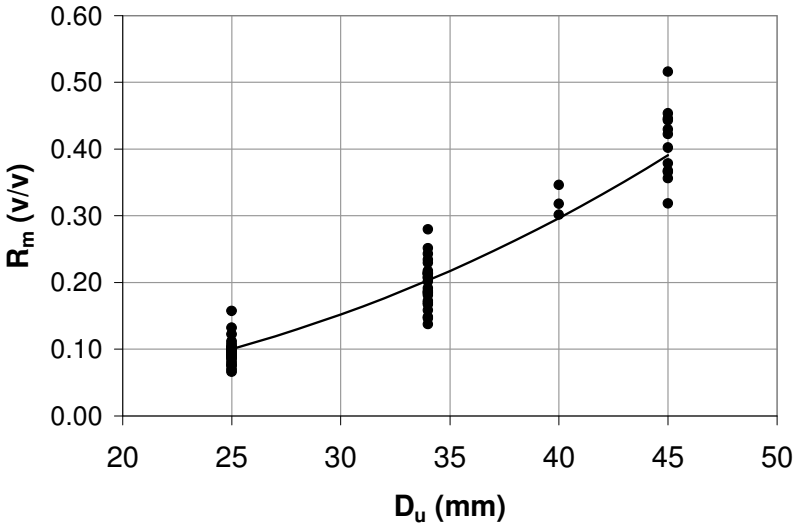

Figure 4.61. The effect of spigot diameter on R_m. (Cone A - 20°)

D_u was also observed to influence the medium density at the sinks. The effect of D_u on the percentage of magnetite particles exiting through the sinks for the cone A is shown in Fig. 4.62. The sinks medium density was diluted as D_u increased.

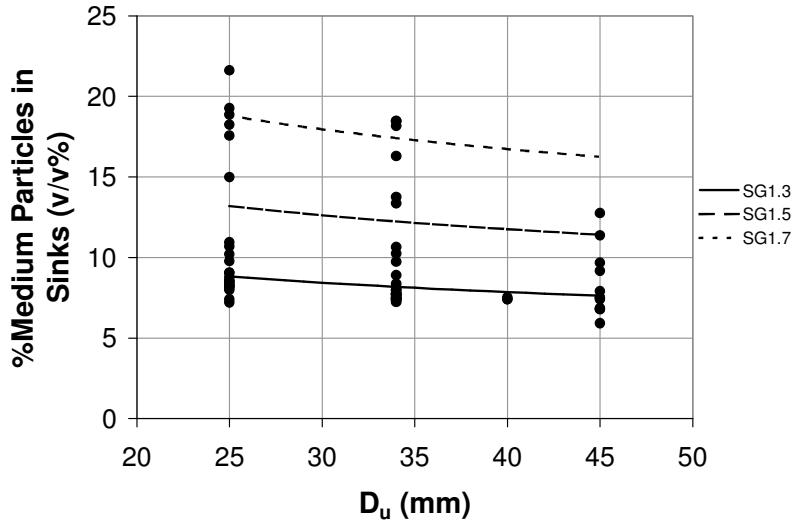

Figure 4.62. Influence of spigot size on volumetric percentage of magnetite particles at the sinks (Cone A –20°).

(c) Vortex Finder Diameter

D_o was observed to influence Q_{USM} in accordance with the following relationship:

$$Q_{USM} \propto D_o^{-0.14}$$

Q_{USM} decreased slightly with increasing D_o, and this is illustrated in Fig. 4.63.

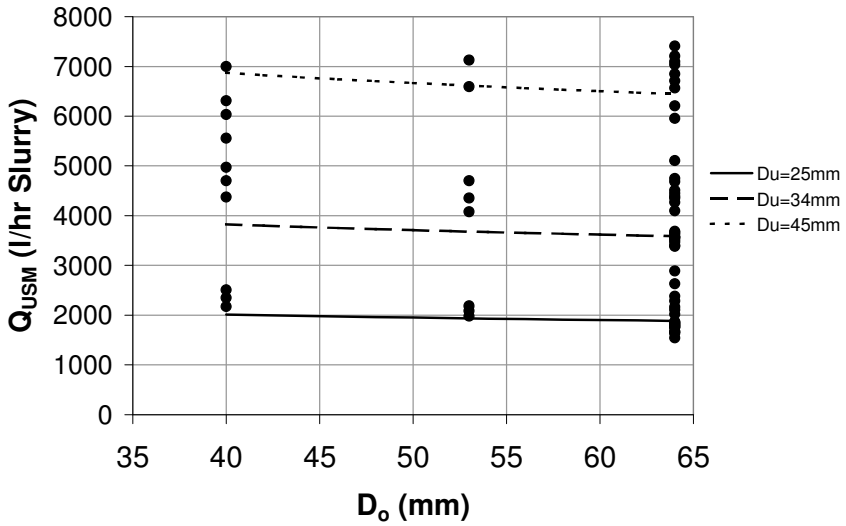

Figure 4.63. The effect of vortex finder diameter on Q_{USM} (Cone A - 20°).

Furthermore, D_o was observed to influence Q_{UM} in accordance with the following relationship:

$$Q_{UM} \propto D_o^{-0.11}$$

Q_{UM} decreased slightly with increasing D_o, and this is illustrated in Fig. 4.64. The effect of D_o on Q_{USM} and Q_{UM} observed in this study is in agreement with the behaviour reported by Stas (1957) that larger spigot-to-vortex finder diameters ratios tend to shift the onset of roping to commence at much higher flow-rates (of slurry and ore) at the sinks.

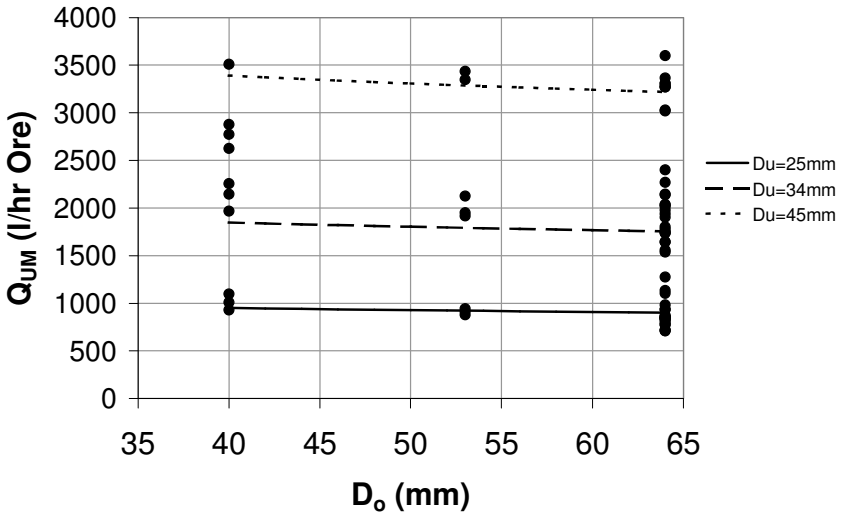

Figure 4.64. The effect of vortex finder diameter on Q_{UM} (Cone A - 20°).

An increase in D_o brought about a slight increase in Q and a decrease in S_R:

$$Q \propto \left(D_u^2 + D_o^2\right)^{0.074}$$

$$S_R = \frac{Q_{USM}}{Q_{OS}} \propto D_o^{-0.25}$$

It is thought that the effect of D_o on Q_{USM} is due to its effect on Q and S_R. Upadrashta and Venkateswarlu (1982), on the other hand, reported S_R to be related to D_o as follows:

$$S_R = \frac{Q_{USM}}{Q_{OS}} \propto D_o^{-2.32}$$

According to Upadrashta and Venkateswarlu, D_o had an equal but opposite effect on S_R as D_u; this behaviour was not observed in the current study. Although D_o and D_u had opposing effects on S_R, their influence on S_R was not in equal in magnitude. Upadrashta and Venkateswarlu (1982) reported S_R to be much more sensitive to D_o than is reported in the current study.

No correlation was found between D_o and C_{mvu}. On the contrary, Fahlstrom (1963) and Heiskanen (2000) observed $\%V_{MSU}$ to increase slightly with increasing D_u/D_o ratio. The

results obtained in the current study seem to suggest that the increase in $\%V_{MSU}$ with increasing D_u/D_o reported by Fahlstrom (1963) and Heiskanen (2000) was probably due to the effect of the spigot diameter only.

Further, R_m was observed to decrease slightly with increasing D_o; the relationship between D_o and R_m found was of the following form:

$$R_m \propto D_o^{-0.25}$$

D_o appears to have a slightly stronger influence on the medium than on the ore particles.

(d) Inlet Size

The inlet size was increased from 70x10 to 70x25 mmxmm; these inlet areas are equivalent to inlet diameters of 30mm (0.2D) and 47mm (0.3D), respectively. The relationship between D_i and Q_{USM} was of the following form:

$$Q_{USM} \propto D_i^{0.43} \quad \text{(Eq. 4.3)}$$

Q_{USM} increased significantly with increasing D_i.

D_i influenced Q_{UM} in accordance with the following relationship:

$$Q_{UM} \propto D_i^{0.38} \quad \text{(Eq. 4.4)}$$

Just as with Q_{USM}, Q_{UM} increased significantly with increasing D_i.

Furthermore, D_i was found to influence Q as follows:

$$Q \propto D_i^{0.90} \quad \text{(Eq. 4.6)}$$

And S_R was observed to be independent of changes in D_i in this study. Thus, the effect of D_i on Q_{USM} and Q_{UM} was due to the increase in Q with increasing D_i. The relationship between Q and D_i obtained in the current study is comparable with those in the literature where the exponent ranged from 1.0 to 1.8 (for dense medium cyclones).

No correlation was found between D_i and C_{mvu}, the same was also true for R_m.

(e) Cyclone Diameter

Cyclone diameter was found to influence Q_{UM} in accordance with the following relationship:

$$Q_{UM} \propto D^{0.63} \quad \text{(Eq. 4.5)}$$

It appears from equation 4.5 that D has a significant and independent effect on Q_{UM}.

(f) Cone Angle

The influence of cone angle on the spigot capacity (Q_{USM} and Q_{UM}) is unclear; the differences in the spigot designs of the 15^o cone and cone A obscured the effect of the cone angle on the spigot capacity. The spigot capacities at the smaller spigot sizes were suppressed by the wall effects, which were enhanced due to the design of the 15^o cone at the spigot as discussed previously. This puts a lot of doubt on whether the behaviour observed in Fig. 4.31 and 4.34 reflects the effect of the cone angle on the spigot capacity, or that of the spigot design as well. Further, an inflection point was encountered in the data obtained with the 15^o cone, while none was observed in the data acquired with 20^o cone angle.

(g) Barrel Length

No correlation was found between Bl, and Q_{USM} and Q_{UM}. Further Q, S_R, C_{mvu}, and R_m were also found to be independent of changes in the barrel length.

4.2.4. Influence of Operational Variables on Spigot Capacity

(a) Feed Pressure

Feed pressure/head was increased only with the 25 and 34mm spigots; at the 45mm spigot diameter the feed head could not be increased significantly due to the constraint on the pump. Q_{USM} was found to be influenced by H as follows.

$$Q_{USM} \propto H^{0.36} \quad \text{(Eq. 4.3)}$$

As expected, Q_{USM} increased with increasing H; the effect of H on Q_{USM} is illustrated in Fig. 4.65.

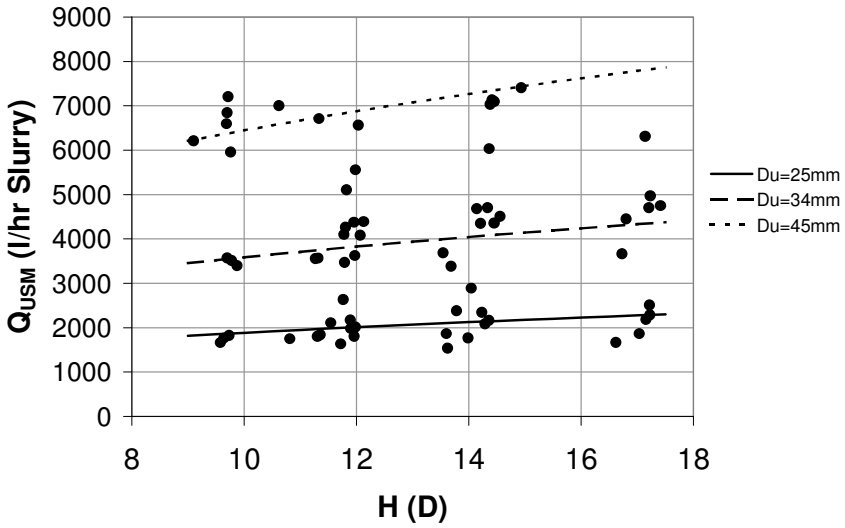

Figure 4.65. The effect of H on Q_{USM}. (165mm cyclone – cone A)

Q_{UM} was found to be influenced by H in accordance with the following relationship:

$$Q_{UM} \propto H^{0.20} \quad \text{(Eq. 4.4)}$$

$$Q_{UM} \propto H^{0.18} \quad \text{(Eq. 4.5)}$$

Q_{UM} increased with increasing H, and the relationship between Q_{UM} and H is shown in Fig. 4.66 and 4.67. This relationship is in good agreement with that reported by DSM, which is as follows:

$$Q_{UM} \propto H^{0.19} \quad \text{(Eq. 2.12)}$$

Van der Walt (1950) also reported the 'maximum permissible spigot loading' that is the spigot capacity, to increase with increasing feed pressure

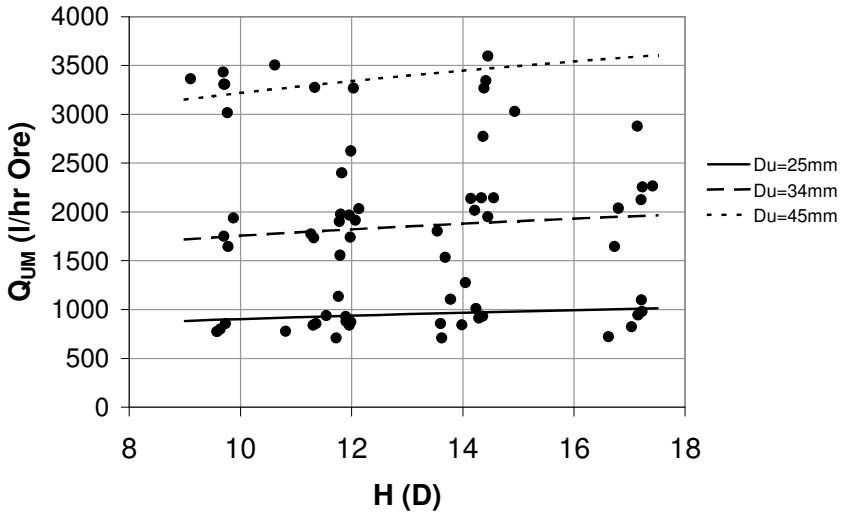

Figure 4.66. The effect of H on Q_{UM}. (165mm cyclone – cone A)

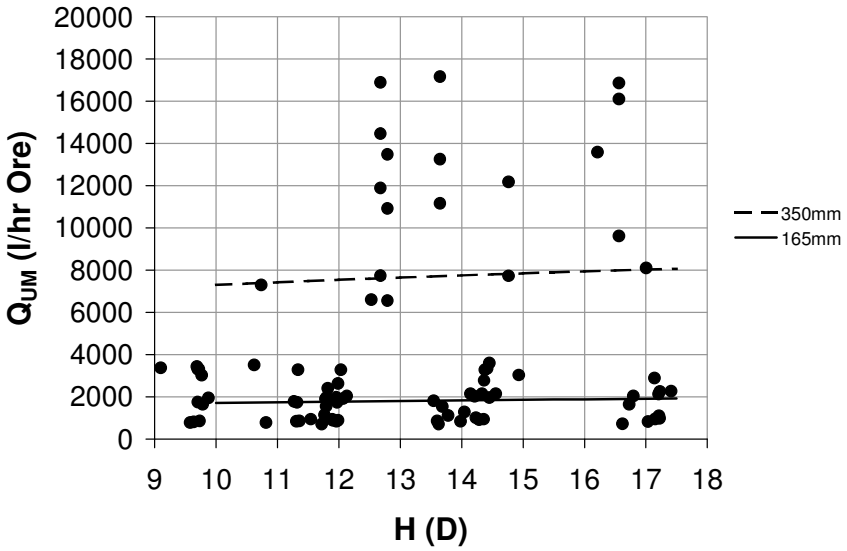

Figure 4.67. The effect of H on Q_{UM}. (350mm cyclone).

It is thought that the effect of H on Q_{USM} and Q_{UM} is a consequence of the influence of H on both Q and S_R:

$$Q \propto H^{0.62} \quad \text{(Eq. 4.6)}$$

$$S_R = \frac{Q_{USM}}{Q_{OS}} \propto H^{-0.70} \quad \text{(Eq. 4.7)}$$

As expected Q increased with increasing H, while S_R decreased with increasing H. Thus, an increase in H increases both the floats and sinks flow-rates, although the floats flow-rate is increased much more strongly than that at the sinks. This accounts for the relatively small influence of H on Q_{USM} and Q_{UM}.

Further, R_m was observed to decrease slightly with increasing D_o; the relationship between D_o and R_m found was of the following form:

$$R_m \propto H^{-0.17} \quad \text{(Eq. 4.10)}$$

The effect of H on R_m appears to be in accordance with the H-Q_{USM} relationship.

The effect of H on C_{mvu} was found not to be statistically significant at the 0.05 significance level.

(b) Medium Density

Q_{USM} decreased with increasing feed medium densities, and the sensitivity of Q_{USM} to ρ_{med} increased significantly at around $\rho_{med} \approx 1.5$RD. Hence, the relationship between Q_{USM} and ρ_{med} was of the following form:

$$Q_{USM} \propto \exp[-5.67(\rho_{med} - 1.45)^3] \quad \text{(Eq. 4.3)}$$

The relationship between feed medium density and Q_{USM} is shown in Fig. 4.68.

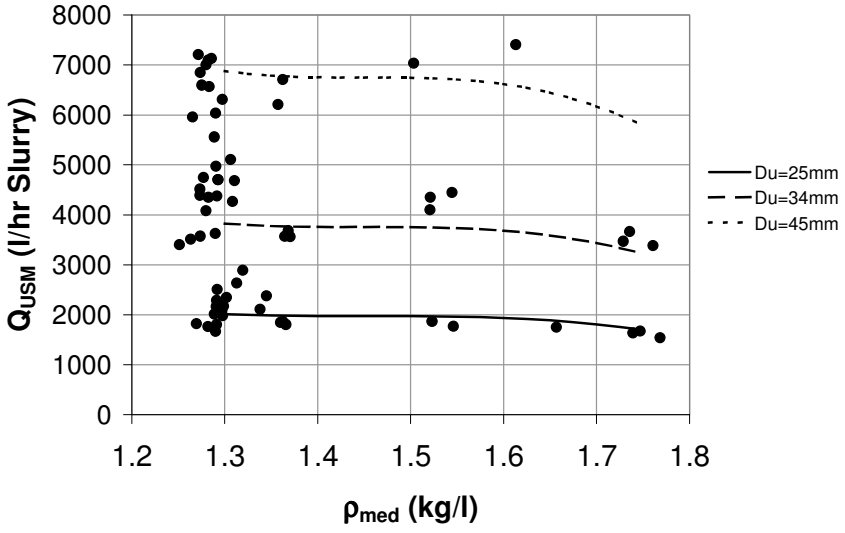

Figure 4.68. The effect of medium density on Q_{USM}. (165mm cyclone – cone A)

Similarly, Q_{UM} was related to the feed medium density in accordance with the following relationship:

$$Q_{UM} \propto \exp[-7.59(\rho_{med} - 1.45)^3] \quad \text{(Eq. 4.4)}$$

Q_{UM} also decreased with increasing ρ_{med} in a similar manner to Q_{USM}; the relationship between ρ_{med} and Q_{UM} is shown in Fig. 4.69.

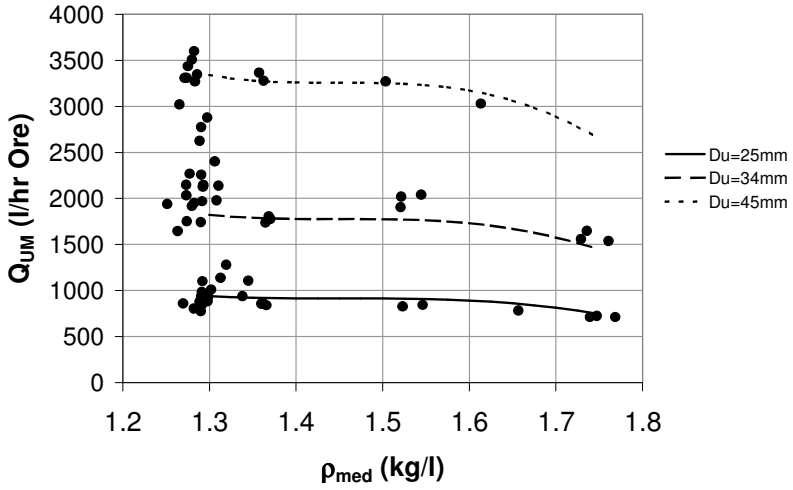

Figure 4.69. The effect of medium density on Q_{UM}. (165mm cyclone –cone A)

Inclusion of the data obtained with the 350mm cyclone in the regression yielded a slightly different relationship:

$$Q_{UM} \propto \exp[-1.58(\rho_{med} - 1.45)^2] \quad \text{(Eq. 4.5)}$$

Q_{UM} increased with increasing ρ_{med} up to a certain critical ρ_{med}, beyond this critical ρ_{med} Q_{UM} decreased with increasing ρ_{med}. This is illustrated in Fig. 4.44 (repeated here for convenience); the plotted lines represent equation 4.5. The best fit was achieved when the value critical ρ_{med} was set at 1.45RD; ρ_{med} values ranging from 1.3 to 1.5 were tried.

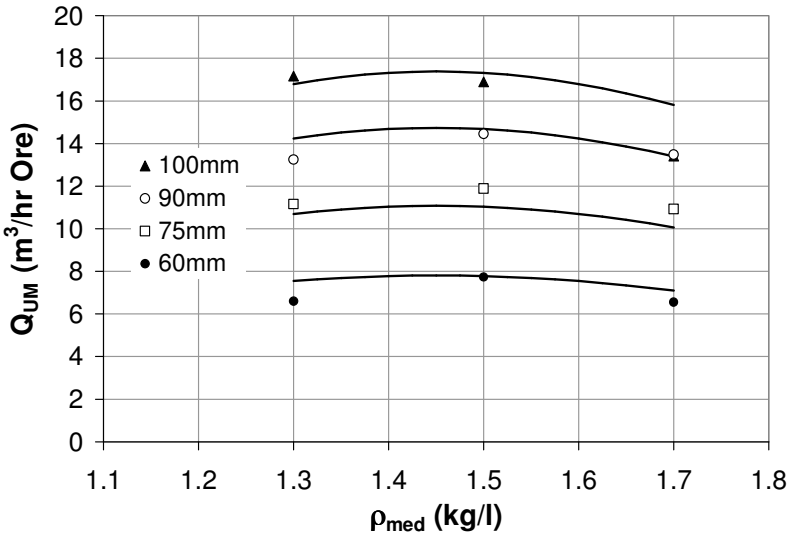

Figure 4.44. The effect of medium density on Q_{UM}. (350mm cyclone)

The effect of ρ_{med} on Q_{USM} and Q_{UM} does not appear to be a consequence of changes in Q and S_R; Q increased with increasing ρ_{med} while S_R was independent of changes in ρ_{med}.

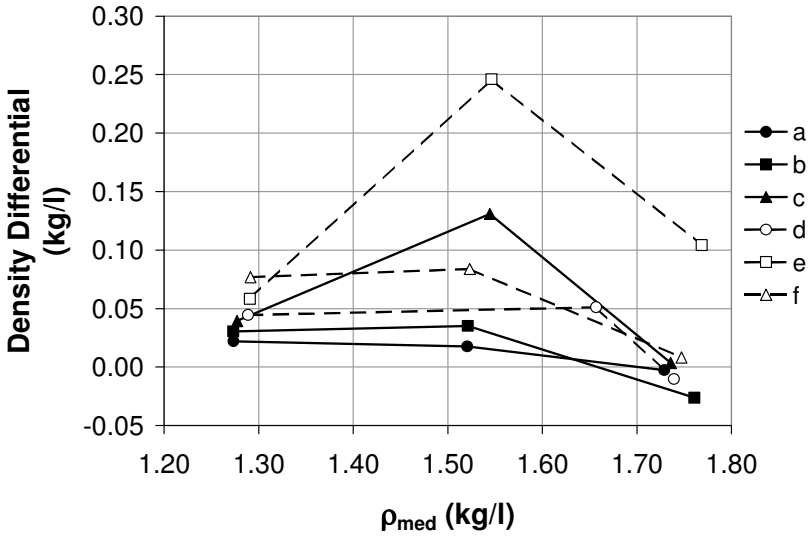

Figure 4.70. The effect of medium density on density differential. (The operating conditions are given in Table A.6 in Appendix A.)

A look at the density differential as ρ_{med} is increased reveals an interesting trend; density differential generally increased with increasing ρ_{med} up to a critical ρ_{med}, beyond which density differential decreased with increasing ρ_{med} (Fig. 4.70). He and Laskowski (1995b), who operated their cyclone with tracers only and magnetite as medium, also reported a similar trend (Fig. 4.71). According to He and Laskowski (1995b), over low medium density ranges

free settling of magnetite particles prevailed and the effect of medium rheology was negligible. While at the high medium density range hindered settling prevailed and the effect of medium rheology was significant. It is thought that the effect of ρ_{med} on Q_{USM} and Q_{UM} is a consequence of changes in the medium rheology with increasing ρ_{med}.

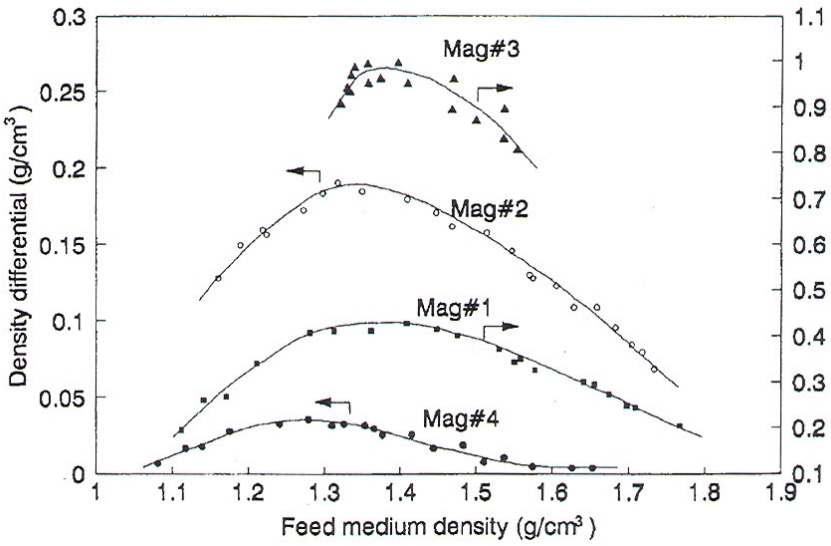

Figure 4.71. The effect of medium density on density differential. (He and Laskowski, 1995b)

The volumetric percent solids in the medium at the sinks with increasing ρ_{med} are shown in Fig. 4.72.

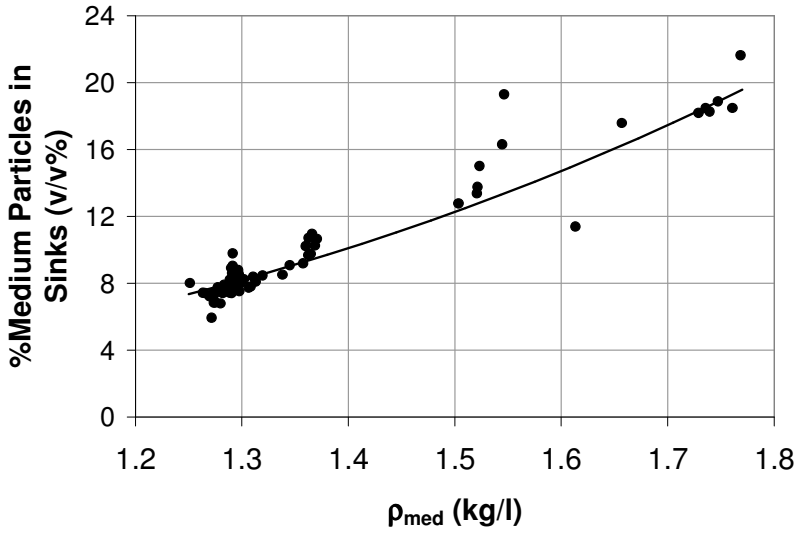

Figure 4.72. Influence of feed medium density on the volumetric percentage of magnetite particles at the sinks.

No correlation was found between medium density and C_{mvu}, the same was also true for R_m. Instead medium density had a strong influence on the volumetric percentage of medium particles exiting at the sinks (Fig. 4.72).

(c) Medium Grade

Medium grade is expressed in terms of percentage magnetite particles passing 45µm. The grade was changed from 95 to 85% passing when operating with cone A; the coarsest magnetite grade was not employed with this cone arrangement. No correlation was found between medium grade and any of the following dependent variables: Q_{USM}, Q_{UM}, Q, S_R and R_m. According to He and Laskowski (1995b) the transition point, beyond which the density differential decreases with increasing ρ_{med}, shifts to higher ρ_{med} values when coarser magnetite medium is used. It is, therefore, expected that medium grade should influence the effect of medium density on Q_{USM} and Q_{UM}. The test-work carried out in the current study was not sufficient to prove or disprove this notion.

Medium grade was, however, found to be poorly correlated to C_{mvu} in accordance with the following relationship:

$$C_{mvu} \propto Gr^{-0.35}$$

C_{mvu} decreased with increasing proportion of the medium particles that were less than 45µm. Thus, the finer the medium particles the lower the C_{mvu} values achieved. This is consistent with the behaviour reported by Plitt et al. (1987) whereby the percent solids at which roping commences decreased with decreasing mass median (50% passing) size of the underflow solids. It is thought that this effect (reported by Plitt et al. and that reported in the current study) is a consequence of increased sensitivity of slurry/medium viscosity to solids concentration when particle sizes are finer. As mentioned previously, it is not unexpected that medium grade should influence spigot overloading behaviour of a dense medium cyclone in a manner that is related/similar to the effect of ore size on the spigot overloading behaviour of a classification cyclone.

(d) Ore Size and Size Distribution

The influence of ore size on the spigot capacity (Q_{USM} and Q_{UM}) is shown in Fig. 4.73 and 4.74; the ore size was changed from –1.8+0.8mm to –5+3mm at vortex finder sizes of 40mm and 64mm. Unfortunately, ore size was changed when operating with the 15° cone, hence it

was not incorporated into equations 4.3 and 4.4. The coarse –5+3mm particles could only be employed with the larger inlet (0.3D) which can take top-sizes of up to 8mm, while the 0.2D inlet can only accommodate a maximum top-size of just over 3mm. All the results shown in Fig. 4.73 and 4.74 were obtained with D_i = 0.3D, and ρ_{med} was maintained at 1.7RD. Q_{USM} and Q_{UM} increased with increasing ore size, although the effect was relatively small at the 25mm spigot. Further, it does not seem as if the influence of particle size on the spigot capacity is related to its influence on Q and S_R. Both of these parameter appear to be unaffected by changes in particle size.

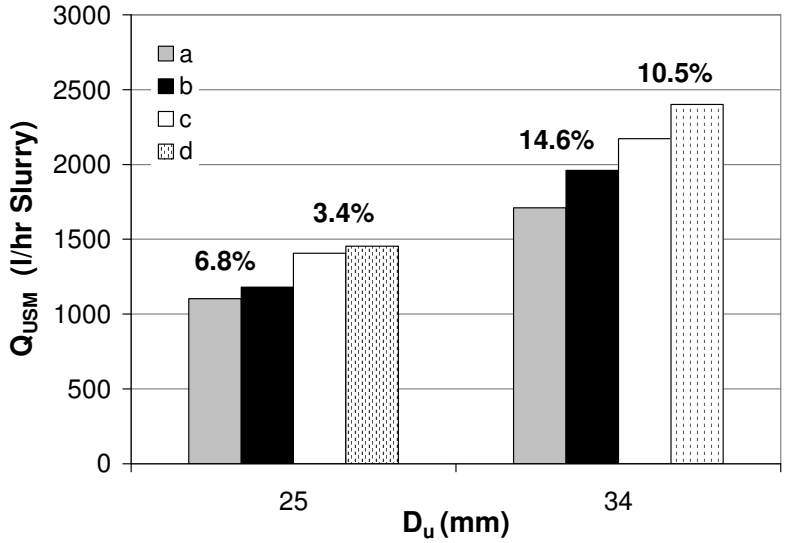

Figure 4.73. The effect of ore size on Q_{USM}. (Full details on the operating conditions are given in Table A.7 in Appendix A).

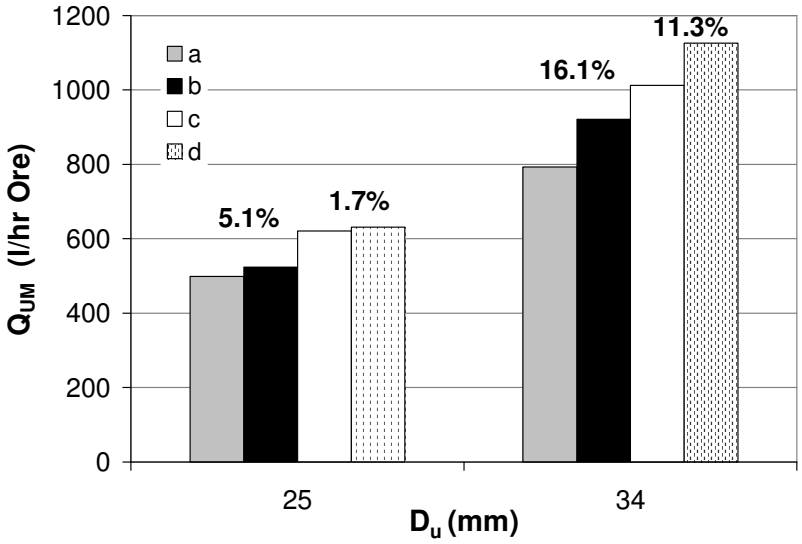

Figure 4.74. The effect of ore size on Q_{UM}. (Full details on the operating conditions are given in Table A.7 in Appendix A).

Ore size did not seem to influence C_{mvu} when the ore size was changed from –1.8+0.8mm to –5+3mm (Fig. 4.75). This was unexpected because it was anticipated that C_{mvu} should be dependent on the packing characteristics of the ore particles. The packing characteristics of the –1.8+0.8mm particles are expected to be considerably different to that of the more coarse –5+3mm particles. This effect is not reflected in Fig. 4.75.

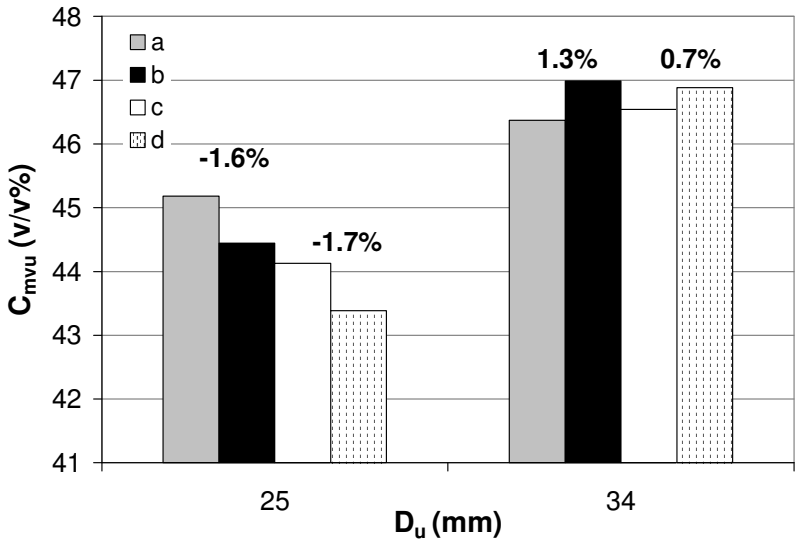

Figure 4.75. The effect of ore size on C_{mvu}. (Full details on the operating conditions are given in Table A.7 in Appendix A).

However, a comparison between the –1.8+0.8mm and the –3+1mm particles indicate that there is a consistent and significant difference between C_{mvu} values obtained for the two size fractions (Fig. 4.78). The –3+1mm size fraction has a wider size distribution than that for the –1.8+0.8mm fraction. It is shown in Fig. 4.78 that –3+1mm size fraction generally obtained higher C_{mvu} values that the –1.8+0.8mm fraction. These observations are in agreement with the findings of Plitt et al. (1987), and Heiskanen (2000) who reported that size distribution of the particles at the underflow to have an effect on the underflow concentration during roping. This, however, did not translate into an increase in Q_{USM} and Q_{UM}, as illustrated in Fig. 4.76 and 4.77. There are strong indications that particle size has an influence on the spigot capacity and none on C_{mvu}, whilst the width of the particle size distribution has no influence on the spigot capacity but has an effect on C_{mvu}.

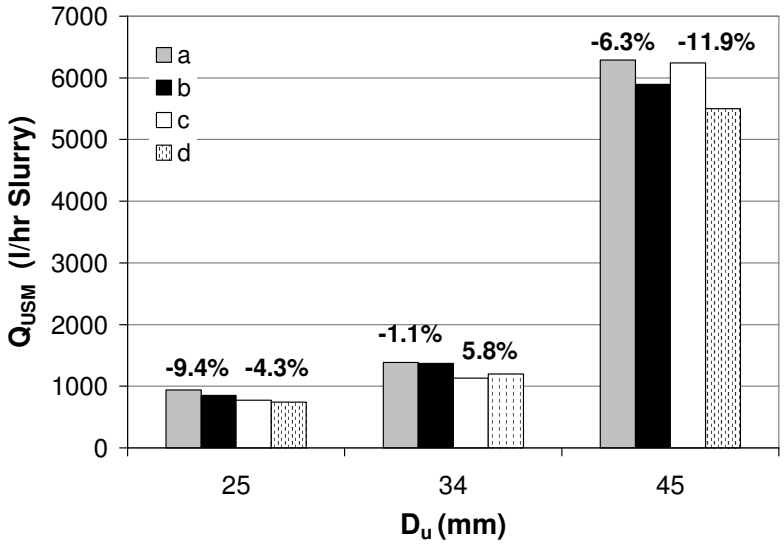

Figure 4.76. The effect of ore size on Q_{USM}: -1.8+0.8mm vs –3+1mm. (Full details on the operating conditions are given in Table A.8 in Appendix A).

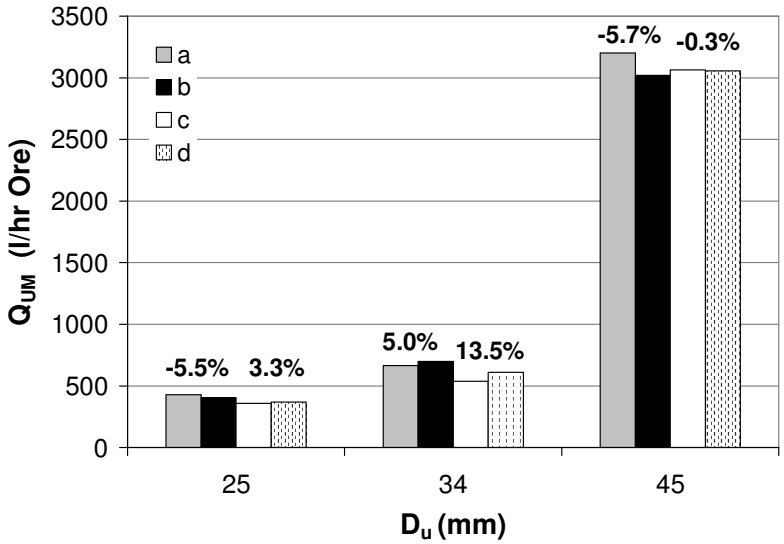

Figure 4.77. The effect of ore size on Q_{UM}: -1.8+0.8mm vs –3+1mm. (Full details on the operating conditions are given in Table A.8 in Appendix A).

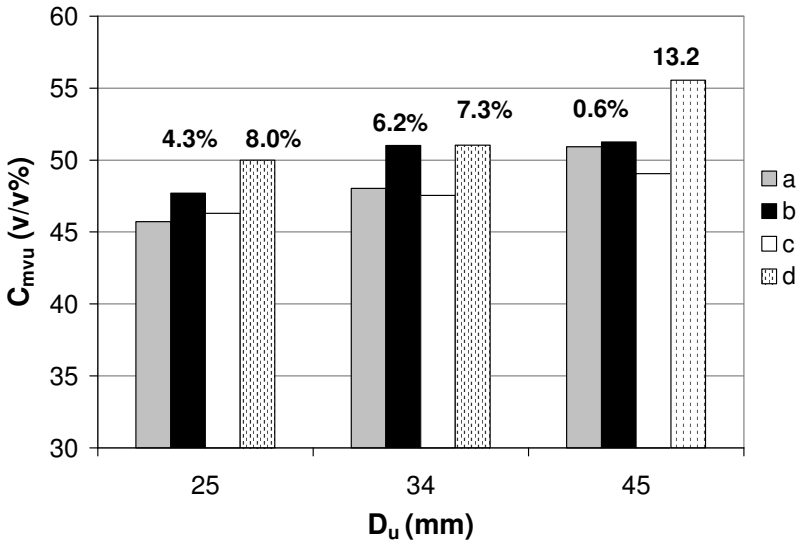

Figure 4.78. The effect of ore size on C_{mvu}: -1.8+0.8mm vs –3+1mm. (Full details on the operating conditions are given in Table A.8 in Appendix A).